

The Hamburg/ESO R-process Enhanced Star survey (HERES) ★ ★★

X. HE 2252–4225, one more r-process enhanced and actinide-boost halo star

L. Mashonkina^{1,2}, N. Christlieb³, and K. Eriksson⁴

¹ Universitäts-Sternwarte München, Scheinerstr. 1, D-81679 München, Germany
e-mail: lyuda@usm.lmu.de

² Institute of Astronomy, Russian Academy of Sciences, RU-119017 Moscow, Russia
e-mail: lima@inasan.ru

³ Zentrum für Astronomie der Universität Heidelberg, Landessternwarte, Königstuhl 12, D-69117 Heidelberg, Germany
e-mail: N.Christlieb@lsw.uni-heidelberg.de

⁴ Department of Astronomy and Space Physics, Uppsala University, Box 515, 75120 Uppsala, Sweden

Received / Accepted

ABSTRACT

Context. Studies of the *r*-process enhanced stars are important for understanding the nature and origin of the *r*-process better.

Aims. We present a detailed abundance analysis of a very metal-poor giant star discovered in the HERES project, HE 2252–4225, which exhibits overabundances of the *r*-process elements with $[r/Fe] = +0.80$.

Methods. We determined the stellar atmosphere parameters, $T_{\text{eff}} = 4710$ K, $\log g = 1.65$, and $[Fe/H] = -2.63$, and chemical abundances by analysing the high-quality VLT/UVES spectra. The surface gravity was calculated from the non-local thermodynamic equilibrium (NLTE) ionisation balance between Fe I and Fe II.

Results. Accurate abundances for a total of 38 elements, including 22 neutron-capture elements beyond Sr and up to Th, were determined in HE 2252–4225. For every chemical species, the dispersion in the single line measurements around the mean does not exceed 0.12 dex. This object is deficient in carbon, as expected for a giant star with $T_{\text{eff}} < 4800$ K. The stellar Na–Zn abundances are well fitted by the yields of a single supernova of $14.4 M_{\odot}$. For the neutron-capture elements in the Sr–Ru, Ba–Yb, and Os–Ir regions, the abundance pattern of HE 2252–4225 is in excellent agreement with the average abundance pattern of the strongly *r*-process enhanced stars CS 22892-052, CS 31082-001, HE 1219-0312, and HE 1523-091. This suggests a common origin of the first, second, and third *r*-process peak elements in HE 2252–4225 in the classical *r*-process. We tested the solar *r*-process pattern based on the most recent *s*-process calculations of Bisterzo, Travaglio, Gallino, Wiescher, and Käppeler and found that elements in the range from Ba to Ir match it very well. No firm conclusion can be drawn about the relationship between the first neutron-capture peak elements, Sr to Ru, in HE 2252–4225 and the solar *r*-process, owing to the uncertainty in the solar *r*-process. The investigated star has an anomalously high Th/Eu abundance ratio, so that radioactive dating results in a stellar age of $\tau = 1.5 \pm 1.5$ Gyr that is not expected for a very metal-poor halo star.

Key words. Stars: abundances – Stars: atmospheres – Stars: fundamental parameters – Nuclear reactions, nucleosynthesis, abundances

1. Introduction

HE 2252–4225 was identified as a candidate metal-poor star in the Hamburg/ESO Survey (HES; see Christlieb et al. 2008, for details of the candidate selection procedures). Moderate-resolution ($\Delta\lambda = 2 \text{ \AA}$) spectroscopy obtained at the Siding Spring Observatory (SSO) 2.3 m-telescope with the Double Beam Spectrograph (DBS) confirmed its metal-poor nature. Therefore, it was included in the target list of the Hamburg/ESO R-process-Enhanced Star survey (HERES). A detailed description of the project and its aims can be found in Christlieb et al. (2004, hereafter Paper I), and the methods of automated abundance analysis of high-resolution “snapshot” spectra are de-

scribed in Barklem et al. (2005, hereafter Paper II). “Snapshot” spectra with a spectral resolution $R \sim 20\,000$ and a signal-to-noise ratio of $S/N \sim 50$ per pixel at 4100 \AA were used to show that HE 2252–4225 is a very metal-poor (VMP) star, with the iron abundance $[Fe/H]^1 = -2.83$, and it exhibits overabundances of the heavy elements produced via rapid neutron captures (*r*-process), with $[Eu/Fe] = +0.99$ and $[Ba/Fe] = +0.45$ (Paper II).

The astrophysical site(s) of the *r*-process is still unclear. Studies of the strongly *r*-process enhanced and VMP stars can provide an empirical information about the origin of the heavy elements beyond the iron group in the early Galaxy. Christlieb et al. (2004) suggest referring to metal-poor stars having $[Eu/Fe] = +0.3$ to $+1.0$ and $[Ba/Eu] < 0$ as r-I stars. Stars with similar $[Ba/Eu]$ abundance ratio, but higher $[Eu/Fe] > +1$, belong to the group of r-II stars. Among a dozen discovered r-II stars, the six stars, CS 22892-052 (Snedden et al. 1994), CS 31082-001 (Cayrel et al. 2001), CS 29497-004 (Paper I),

Send offprint requests to: L. Mashonkina; e-mail: lima@inasan.ru

* Based on observations collected at the European Southern Observatory, Paranal, Chile (Proposal numbers 170.D-0010, and 280.D-5011).

** Table 3 is only available in electronic form at the CDS via anonymous ftp to cdsarc.u-strasbg.fr (130.79.128.5) or via http://cdsweb.u-strasbg.fr/cgi-bin/qcat?J/A+A/

¹ In the classical notation, where $[X/Y] = \log(N_X/N_Y)_{\text{star}} - \log(N_X/N_Y)_{\text{sun}}$.

HE 1219-0312 (Paper II), HE 1523-091 (Frebel et al. 2007), and SDSS J2357-0052 (Aoki et al. 2010), are extremely enhanced in the *r*-process elements, with $[\text{Eu}/\text{Fe}] \geq 1.5$. Their heavy-element abundances are expected to be dominated by the influence of a single event, or at most very few *r*-process nucleosynthesis events.

It was established that *r*-II and *r*-I stars have a very similar heavy-element abundance pattern in the Ba–Hf region that, in turn, is consistent with a scaled solar system (SS) *r*-process abundance distribution (see for example Sneden et al. 2008, Cowan et al. 2002, Ivans et al. 2006, Sitnova & Mashonkina 2011, Siqueira-Mello et al. 2014). This suggests a universal production ratio of the second *r*-process peak elements during the Galaxy history. A different case is the light trans-iron elements. Observations of MP halo stars appear to infer a distinct production mechanism for Sr–Zr and heavy elements beyond Ba in the early Galaxy (Aoki et al. 2005, François et al. 2007, Mashonkina et al. 2007b). Mashonkina et al. (2010) found a clear distinction in Sr/Eu abundance ratios between the *r*-II and *r*-I stars, namely, the *r*-II stars contain a low Sr/Eu abundance ratio at $[\text{Sr}/\text{Eu}] = -0.92 \pm 0.13$, while the *r*-I stars have 0.36 dex higher Sr/Eu values.

In this paper, we investigate whether the heavy-element abundance pattern of HE 2252–4225 matches that of the extremely neutron-capture-rich *r*-II stars. What is the behaviour of the first *r*-process peak elements from Sr to Pd in HE 2252–4225? Can a nucleo-chronometric age of HE 2252–4225 be estimated from measurement of the radioactive element thorium? How can an abundance analysis of HE 2252–4225 improve our knowledge of the *r*-process? To answer these questions, we continue our series of papers on the HERES project and aim to revise stellar parameters and to perform detailed abundance analysis of HE 2252–4225, based on the high-quality VLT/UVES spectra and refined theoretical methods of line-formation modelling.

This paper is structured as follows. After presenting the observations in Sect. 2, we describe our determination of stellar parameters and abundance analysis of HE 2252–4225 in Sects. 3 and 4. Section 5 analyses the heavy element abundance pattern of the investigated star. An anomalously high Th abundance of HE 2252–4225 is discussed in Sect. 6. Our conclusions are presented in Sect. 7.

2. Observations

For the convenience of the reader, we list the coordinates and photometry of HE 2252–4225 in Table 1. The photometry was taken from Beers et al. (2007). High-quality spectra of this star was acquired during May–September 2005 with the VLT and UVES in dichroic mode. The BLUE390+RED580 (9 h total integration time), and BLUE437+RED860 (10 h) standard settings were employed to ensure a wide wavelength coverage. The slit width of $0.8''$ in both arms yielded a resolving power of $R = 50\,000$. A 1×1 pixel binning ensured proper sampling of the spectra. The observations are summarised in Table 2.

The pipeline-reduced spectra were shifted to the stellar rest frame and then co-added in an iterative procedure in which we identified pixels in the individual spectra affected by cosmic ray hits that had not been fully removed during the data reduction, or those affected by CCD defects or other artefacts. These pixels were flagged and ignored in the final iteration of the co-addition. Both sets of co-added blue spectra have S/N of at least 50 per pixel at $\lambda > 3800 \text{ \AA}$. At the shortest wavelengths, the S/N of the

BLUE390 and BLUE437 is 10 (at 3400 \AA) and 70 (at 3756 \AA), respectively. The red arm spectra have $S/N > 100$ per pixel in most of the covered spectral range.

Table 1. Coordinates and photometry of HE 2252–4225.

R.A.(2000.0)	22:54:58.6
dec.(2000.0)	−42:09:19
<i>V</i>	14.878 ± 0.003
<i>B</i> − <i>V</i>	0.822 ± 0.005
<i>V</i> − <i>R</i>	0.499 ± 0.005
<i>V</i> − <i>I</i>	1.023 ± 0.006

Table 2. VLT/UVES observations of HE 2252–4225.

Setting	λ^1	t_{exp}	S/N^2
BLUE390	3400–4515 Å	8.9 h	10–65
BLUE437	3765–4985 Å	10.0 h	70–120
REDL580	4795–5760 Å	8.9 h	100–120
REDU580	5845–6810 Å	8.9 h	60–120
REDL860	8400–8526 Å	10.0 h	100–180

Notes. ¹ λ refers to rest frame wavelengths,

² S/N refers to the signal-to-noise ratio per pixel.

3. Stellar atmosphere parameters

In Paper II, an effective temperature of $T_{\text{eff}} = 4708 \pm 100 \text{ K}$ was determined from photometry when adopting the reddening derived from the maps of Schlegel et al. (1998). A subsequent analysis of the snapshot spectrum inferred that HE 2252–4225 is a VMP giant with the surface gravity $\log g = 1.53 \pm 0.24$, $[\text{Fe}/\text{H}] = -2.83 \pm 0.12$ and the microturbulence velocity $\xi_t = 1.9 \pm 0.1 \text{ km s}^{-1}$. These parameters appear to be close to those of HD 122563, which is one of the best observed halo stars, with well-determined T_{eff} and $\log g$. Recent measurements of the angular diameter of HD 122563 resulted in $T_{\text{eff}} = 4600 \pm 41 \text{ K}$ (Creevey et al. 2012). Employing the same T_{eff} , Mashonkina et al. (2011) calculated $\log g = 1.60 \pm 0.07$ from the HIPPARCOS parallax and $[\text{Fe}/\text{H}] = -2.56$ from the NLTE analysis of the Fe lines. We found that HE 2252–4225 and HD 122563 have very similar line profiles for $\text{H}\alpha$ and $\text{H}\beta$ (Fig. 1, top panel displays only $\text{H}\beta$). This confirms that HE 2252–4225 is indeed cool, and its effective temperature may be only slightly higher than that of HD 122563. The high-quality spectrum of HD 122563 ($R \simeq 80\,000$ and $S/N > 200$) was taken from the ESO UVESPOP survey (Bagnulo et al. 2003).

In this study, we check $T_{\text{eff}} = 4710 \text{ K}$ through a profile analysis of $\text{H}\alpha$ and $\text{H}\beta$ and revise the surface gravity, iron abundance, and microturbulence velocity using lines of Fe I and Fe II. $\text{H}\gamma$ was not used due to heavy blending of the line wings. Our calculations are based on non-local thermodynamic equilibrium (NLTE) line formation for H I and Fe I–II, employing the methods described by Mashonkina et al. (2008) and Mashonkina et al. (2011), respectively. The coupled radiative transfer and statistical equilibrium (SE) equations were solved with a revised version of the DETAIL code (Butler & Giddings 1985). The update was presented by Mashonkina et al. (2011). The obtained departure coefficients were then used by the code SIU (Reetz 1991) to calculate the synthetic line profiles.

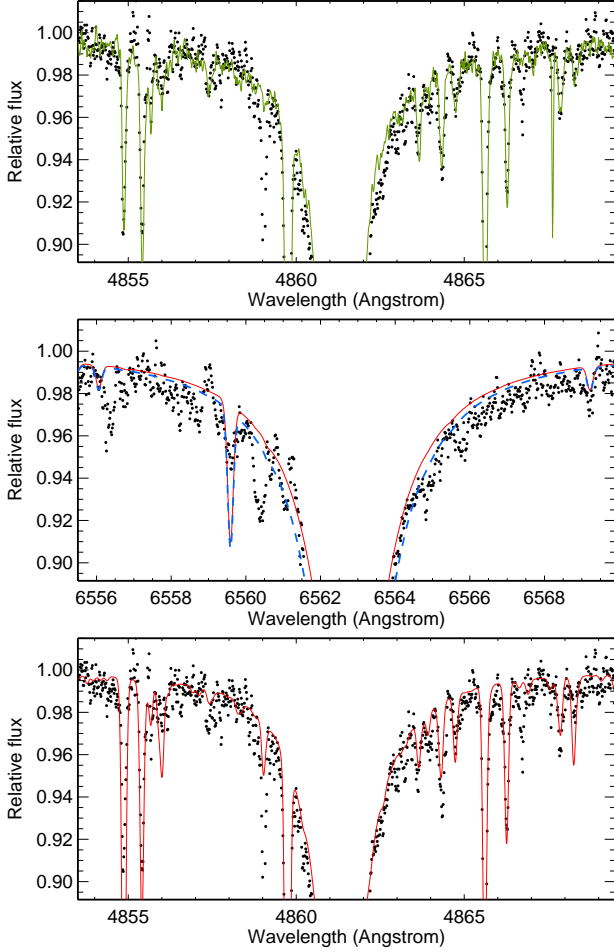


Fig. 1. Top panel: observed profiles of H β in HE 2252–4225 (bold dots) and HD 122563 (continuous curve). Middle and bottom panels: synthetic NLTE (continuous curve) and LTE (dashed curve) flux profile of H α and H β computed for $T_{\text{eff}} = 4710$ K compared to the observed spectrum of HE 2252–4225 (bold dots). In all calculations, $\log g = 1.65$, $[\text{Fe}/\text{H}] = -2.66$, and $\xi = 1.7 \text{ km s}^{-1}$.

When determining the stellar parameters of HE 2252–4225, we used the MARCS model structures (Gustafsson et al. 2008)², which were interpolated for given T_{eff} , $\log g$, and $[\text{Fe}/\text{H}]$ using a FORTRAN-based routine written by Thomas Masseron³.

3.1. Effective temperature

The Balmer lines were computed for a small grid of model atmospheres with common $T_{\text{eff}} = 4710$ K, but varying gravity, with $\log g = 1.2, 1.53, 1.65$, and 1.75 , and metallicity, with $[\text{M}/\text{H}] = -2.5, -2.66, -2.83$, and -3.0 . The theoretical profiles were obtained by convolving the profiles resulting from the thermal, natural, and Stark broadening (Vidal et al. 1973), as well as self-broadening (Barklem et al. 2000). In the SE calculations, inelastic collisions with hydrogen atoms were accounted for using the classical Drawin rates (Drawin 1968, 1969) scaled by a factor of $S_{\text{H}} = 2$, as recommended by Mashonkina et al. (2008). It was found that a variation in $\log g$ and $[\text{M}/\text{H}]$ within 0.24 dex and

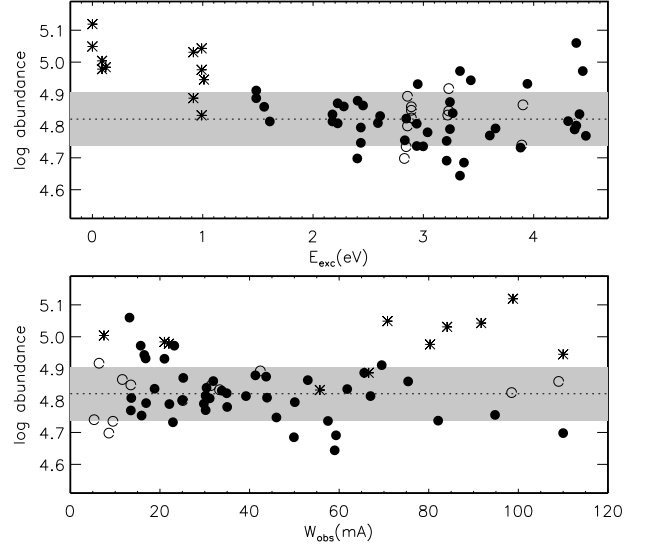


Fig. 2. Trends of NLTE abundances with excitation potential and equivalent width, as determined from individual Fe I (filled circles for $E_{\text{exc}} \geq 1.2$ eV and asterisks for $E_{\text{exc}} < 1.2$ eV) and Fe II (open circles) lines, using our adopted stellar parameters. The dotted line indicates the mean Fe abundance from two ionisation stages and the shaded grey area its statistical error.

0.12 dex, respectively, produces minor effect on the H α and H β profiles, such that the difference in derived T_{eff} does not exceed 30 K. Figure 1 displays observed profiles of the two Balmer lines in HE 2252–4225 compared with the theoretical NLTE and LTE (only for H α) ones calculated for $\log g = 1.65$ and $[\text{Fe}/\text{H}] = -2.66$. The departures from LTE are weak for the H β profile beyond the core, such that the difference between T_{eff} derived for this line, assuming either NLTE or LTE, does not exceed 30 K. For both lines, the observed wings are satisfactorily reproduced by the model atmosphere with $T_{\text{eff}} = 4710$ K, and this value was adopted as a final effective temperature of HE 2252–4225.

3.2. Surface gravity, iron abundance, and microturbulence velocity

The lines employed to determine $\log g$, $[\text{Fe}/\text{H}]$, and ξ_t were mainly selected from the linelist produced in our previous HERES paper (Mashonkina et al. 2010, hereafter, Paper V). They are listed in Table 3 (online material), along with transition information, references for the adopted gf -values, and the final element abundances. The LTE and NLTE abundances were calculated for the four model atmospheres, with common $T_{\text{eff}} = 4710$ K and $[\text{M}/\text{H}] = -2.83$, but various $\log g = 1.20, 1.53, 1.65$, and 1.75 and $\xi_t = 1.7, 1.9$, and 2.1 km s^{-1} . In the atmospheres of MP stars, the main source of uncertainties in NLTE results is poorly known inelastic collisions with H I atoms. Therefore, the two sets of NLTE abundances corresponding to $S_{\text{H}} = 0.1$ and $S_{\text{H}} = 1$ were computed for each model. Figure 2 displays the NLTE ($S_{\text{H}} = 0.1$) abundances from individual lines of Fe I and Fe II in the model $T_{\text{eff}}/\log g/[\text{M}/\text{H}]/\xi_t = 4710/1.65/-2.66/1.7$.

We found that the low-excitation lines ($E_{\text{exc}} < 1.2$ eV) of Fe I give systematically higher abundances compared with the mean from the remaining lines, independent of either LTE or

² <http://marcs.astro.uu.se>

³ <http://marcs.astro.uu.se/software.php>

Table 4. Determined stellar parameters of HE 2252–4225.

Parameter	Value	Uncertainty
T_{eff}	4710 K	± 100 K
$\log g$	1.65	± 0.15
[Fe/H]	-2.63	± 0.08
ξ_t	1.7 km s ⁻¹	± 0.1 km s ⁻¹

NLTE and independent of the used ξ_t and $\log g$. For example, in the model 4710/1.65/-2.66/1.7, the abundance difference between the $E_{\text{exc}} < 1.2$ eV and $E_{\text{exc}} > 1.2$ eV lines of Fe I amounts to 0.19 dex in NLTE ($S_{\text{H}} = 0.1$) and 0.21 dex in LTE. This can be caused by ignoring hydrodynamic phenomena (3D effects) in the atmosphere of HE 2252–4225. Collet et al. (2007), Hayek et al. (2011), and Dobrovolskas et al. (2013) predicted that the (3D-1D) abundance corrections are negative for lines of Fe I in the $[M/H] = -2$ and -3 models of VMP cool giants and the magnitude of the correction depends strongly on excitation energy of the lower level. For example, in the 4858/2.2/-3 model, (3D-1D) = -0.8 dex and -0.05 dex for the $E_{\text{exc}} = 0$ and 4 eV lines, respectively (Hayek et al. 2011). We do not see such a large discrepancy between the low- and high-excitation lines of Fe I in HE 2252–4225. Nevertheless, we excluded lines with $E_{\text{exc}} < 1.2$ eV, when calculating the mean abundance and analysing the abundance trend with the line strength for Fe I.

It was found that a variation of 0.2 km s⁻¹ in ξ_t led to a similar change of 0.03 dex in the derived mean abundances from Fe I and Fe II lines, therefore, the gravity determination did not depend on the adopted value of ξ_t . However, including the results for $\xi_t = 2.1$ km s⁻¹ produced a steep trend with observed equivalent widths, W_{obs} , for the abundances found from individual Fe I and Fe II lines, independent of the adopted values of $\log g$. The least slope of the $\log \varepsilon_{\text{Fe}} - W_{\text{obs}}$ plot was obtained with $\xi_t = 1.7$ km s⁻¹.

Consistent iron abundances for the two ionisation stages were obtained with $\log g = 1.2$ in LTE, $\log g = 1.35$ in NLTE with $S_{\text{H}} = 1$, and $\log g = 1.65$ in NLTE with $S_{\text{H}} = 0.1$. The discrepancy in LTE gravity between this study and Paper II can be explained by using different sources of gf -values for Fe II lines and a different list of the Fe lines in the two studies. The present results are based on recent gf -values of Meléndez & Barbuy (2009). When choosing between $S_{\text{H}} = 1$ and 0.1, we relied on an analysis of iron lines in HD 122563, where applying $S_{\text{H}} = 0.1$ led to consistent NLTE abundances for Fe I and Fe II for the gravity calculated from the HIPPARCOS parallax (Mashonkina et al. 2011). Thus, $\log g = 1.65$ was adopted as a final surface gravity of HE 2252–4225. The uncertainty in $\log g$ was estimated as 0.15 dex based on the statistical errors of the mean abundances for Fe I, $\log \varepsilon_{\text{FeI}} = 4.79 \pm 0.09$, and Fe II, $\log \varepsilon_{\text{FeII}} = 4.79 \pm 0.07$. We refer to abundances on the usual scale, where $\log \varepsilon_{\text{H}} = 12$. Hereafter, the statistical error is the dispersion in the single line measurements around the mean: $\sigma_{\log \varepsilon} = \sqrt{\sum (\bar{x} - x_i)^2 / (N_{\text{lines}} - 1)}$.

We did not use the ionisation equilibrium between Ca I and Ca II to constrain the gravity because the observed Ca II 3933 Å and 8498 Å lines are very strong, with $W_{\text{obs}} = 5848$ mÅ and 509 mÅ, respectively, and they cannot be accurately measured due to the uncertainty in continuum normalisation. Furthermore, Ca II 8498 Å is insensitive to surface gravity variation. The difference in abundance from Ca II 8498 Å amounts to -0.03 dex between $\log g = 1.20$ and 1.53, and it is smaller than 0.01 dex between $\log g = 1.53$, 1.65, and 1.75.

The obtained parameters $T_{\text{eff}} = 4710$ K, $\log g = 1.65$, $[\text{Fe}/\text{H}] = -2.66$, and $\xi = 1.7$ km s⁻¹ were employed to compute the final model atmosphere with the code MARCS. Enhancements of the α -elements O, Mg, Si, and Ca were adopted to be typical of galactic halo stars, with $[\alpha/\text{Fe}] = 0.4$. We found that moving from the interpolated to an explicitly tailored model atmosphere does not require any revision in derived surface gravity and microturbulence velocity, and the mean NLTE abundances from lines of Fe I and Fe II increase by a similar and small amount of 0.03 dex. With the new model atmosphere, they equal $\log \varepsilon_{\text{FeI}} = 4.82 \pm 0.08$ and $\log \varepsilon_{\text{FeII}} = 4.82 \pm 0.07$. We also checked lines of CH, Ca I, and Ba II. For the atomic lines, the difference nowhere exceeds 0.03 dex. However, the use of the interpolated model leads to a 0.08 dex lower C abundance from the CH molecular lines. The adopted stellar parameters of HE 2252–4225 are given in Table 4. The investigated star is, most probably, a distant object, with a spectroscopic distance of 12.6 kpc, as estimated assuming a stellar mass of 0.8 solar mass.

4. Abundance analysis

Our determinations of the elemental abundances are based on line-profile and equivalent-width analyses, using the codes SIU (Reetz 1991) and WIDTH9⁴ (Kurucz 2005), respectively. The SIU and WIDTH9 codes both treat continuum scattering correctly; i.e., scattering is taken into account not only in the absorption coefficient, but also in the source function.

The lines used in the abundance analysis are listed in Table 3 (online material), along with the transition information and references to the adopted gf -values. They were mostly selected from the list produced in Paper V. The data from Paper V were replaced with gf -values from recent laboratory measurements for Ti I (Lawler et al. 2013), Ti II (Wood et al. 2013), Mn I (Den Hartog et al. 2011), and Zn I (Roederer & Lawler 2012), where available. Hyper-fine splitting (HFS) and/or isotopic splitting (IS) structure were accounted for properly for the lines of chemical elements that are represented by either a single isotope with an odd number of nucleons or multiple isotopes. Table 3 (online material) provides notes that indicate whether HFS/IS was considered in a given feature, and references to the HFS/IS data used. For Mn I levels, we used magnetic dipole constants A from Table 1 in Lefèbvre et al. (2003). The method of calculations and adopted isotope abundances were described in detail in Paper V. We ignored any lines with equivalent widths larger than 100 mÅ. Exceptions were the elements, such as strontium, for which only strong lines can be detected in HE 2252–4225.

Owing to the high-quality and broad wavelength coverage of the spectra used in this study, we derived the abundance of 38 elements from C to Th in HE 2252–4225 and, for 22 elements of them, in the nuclear charge range between $Z = 38$ and 90. The oxygen, copper, and hafnium abundances could not be determined from the available observed spectrum. We were unsuccessful in obtaining abundances for Rh and Pd, because the strongest lines of these elements, Rh I 3434 Å and Pd I 3404 Å, could not be extracted from the noise in the $S/N \approx 15$ observed spectrum of HE 2252–4225. The element abundances obtained from individual lines are listed in Table 3 (online material). For each feature, we provide the LTE abundance and, for selected species, also the NLTE abundance. Table 5 presents the mean abundances, the number of used lines, N_{lines} , and $\sigma_{\log \varepsilon}$, where $N_{\text{lines}} > 1$. We also list the solar photosphere abundances, $\log \varepsilon_{\odot}$, adopted from Lodders et al. (2009), and the abundances relative

⁴ <http://kurucz.harvard.edu/programs/WIDTH/>

Table 5. Summary of the abundances of HE 2252–4225.

Z	Species	$\log \varepsilon_{\odot}$	N_{lines}	$\log \varepsilon$	$\sigma_{\log \varepsilon}$	[X/Fe]
3	Li I	1.10	1	≤ -0.1	–	
6	CH	8.39	4	5.15	0.02	–0.61
7	NH	7.86	1	4.91		–0.32
11	Na I	6.30	2	3.13^N	0.00	–0.54
12	Mg I	7.54	3	5.09^N	0.12	0.18
13	Al I	6.47	1	2.99^N		–0.85
14	Si I	7.52	1	4.97^N		0.08
20	Ca I	6.33	10	3.92^N	0.06	0.22
21	Sc II	3.07	4	0.32	0.05	–0.12
22	Ti I	4.90	10	2.26	0.06	0.25
22	Ti II	4.90	16	2.64	0.09	0.37
23	V II	4.00	3	1.12	0.03	–0.25
24	Cr I	5.64	5	2.66	0.06	–0.09
24	Cr II	5.65	4	3.05	0.05	0.03
25	Mn I	5.37	3	2.41	0.05	–0.07
25	Mn II	5.37	3	2.62	0.02	–0.12
26	Fe I	7.45	43	4.82^N	0.08	0.00
26	Fe II	7.45	12	4.82^N	0.07	0.00
27	Co I	4.92	3	2.00	0.08	–0.03
27	Co II	4.92	1	2.16		–0.13
28	Ni I	6.23	6	3.36	0.11	0.02
28	Ni II	6.23	1	3.75		0.15
30	Zn I	4.62	2	2.42^T	0.01	0.43
38	Sr II	2.92	2	0.16	0.00	–0.13
38	Sr II	2.92	2	0.20^N	0.05	–0.09
39	Y II	2.21	9	–0.56	0.11	–0.14
40	Zr II	2.58	12	0.07	0.07	0.12
42	Mo I	1.92	1	–0.84		0.13
44	Ru I	1.84	1	–0.45		0.60
56	Ba II	2.17	3	–0.17	0.08	0.29
56	Ba II	2.17	3	-0.32^N	0.04	0.14
57	La II	1.14	8	–1.09	0.06	0.40
58	Ce II	1.61	10	–0.73	0.03	0.29
59	Pr II	0.76	3	–1.26	0.03	0.61
60	Nd II	1.45	19	–0.61	0.07	0.57
62	Sm II	1.00	5	–0.90	0.01	0.73
63	Eu II	0.52	4	–1.30	0.02	0.81
63	Eu II	0.52	4	-1.20^N	0.03	0.91
64	Gd II	1.11	4	–0.77	0.06	0.75
65	Tb II	0.28	3	–1.56	0.00	0.79
66	Dy II	1.13	14	–0.58	0.09	0.92
67	Ho II	0.51	4	–1.29	0.07	0.83
68	Er II	0.96	8	–0.89	0.09	0.78
69	Tm II	0.14	5	–1.76	0.05	0.73
70	Yb II	0.86	1	–0.91		0.86
76	Os I	1.45	1	–0.44		0.74
77	Ir I	1.38	2	–0.31	0.10	0.94
82	Pb I	2.00	1	≤ -0.78	0.30	≤ -0.15
82	Pb I	2.00	1	$\leq -0.37^N$	0.30	≤ 0.26
90	Th II	0.08	2	–1.63	0.02	0.92
90	Th II	0.08	2	-1.55^N	0.01	1.00

Notes. ^(N) NLTE abundance;^(T) NLTE correction from Takeda et al. (2005).

to iron, [X/Fe]. For computing [X/Fe], $[\text{Fe}/\text{H}]_{\text{NLTE}} = -2.63$ was chosen as the reference, with the exception of the neutral species calculated based on a LTE assumption, where the reference is $[\text{Fe I}/\text{H}]_{\text{LTE}} = -2.89$. Figure 3 displays the element abundance pattern of HE 2252–4225.

4.1. NLTE effects

NLTE abundances were derived for a number of chemical species, using the NLTE methods from Alexeeva et al. (2014, Na I), Mashonkina (2013, Mg I), Baumüller & Gehren (1996, Al I), Shi et al. (2008, Si I), Mashonkina et al. (2007a, Ca I), Belyakova & Mashonkina (1997, Sr II), Mashonkina et al. (1999, Ba II), Mashonkina & Gehren (2000, Eu II, updated), and Mashonkina et al. (2012, Pb I, Th II). Quantum-mechanical rate coefficients from Barklem et al. (2010) and Barklem et al. (2012) were applied for Na+H and Mg+H collisions, respectively. For the remaining NLTE species, collisions with H I atoms were computed with the Drawin rates (Drawin 1968, 1969) scaled by a factor of $S_{\text{H}} = 0.1$. An exception is Sr II and Ba II, for which $S_{\text{H}} = 0.01$ was adopted, as recommended by Mashonkina & Gehren (2001).

We calculated that the NLTE abundances derived from the Na I 5890 and 5896 Å lines are –0.44 dex lower than the corresponding LTE values. In contrast, the NLTE abundance correction, $\Delta_{\text{NLTE}} = \log \varepsilon_{\text{NLTE}} - \log \varepsilon_{\text{LTE}}$, is positive for lines of Mg I, Al I, and Ca I. For Ca I, $\Delta_{\text{NLTE}} = 0.24$ dex, on average. The departures from LTE are small for Mg I 4703 and 5528 Å, with $\Delta_{\text{NLTE}} = 0.03$ and 0.01 dex, respectively. A small negative correction of $\Delta_{\text{NLTE}} = -0.02$ dex was calculated for Si I 3905 Å.

Evidence of notable departures from LTE was obtained for Ti I, Cr I, Mn I, Co I, and Ni I. Each of the corresponding elements is observed in HE 2252–4225 for two ionisation stages, and the LTE abundance derived from lines of the neutrals is lower than that for the first ions with the following differences:

$$\begin{aligned} \Delta \log \varepsilon(\text{Ti I} - \text{Ti II}) &= -0.38 \text{ dex}, \\ \Delta \log \varepsilon(\text{Cr I} - \text{Cr II}) &= -0.39 \text{ dex}, \\ \Delta \log \varepsilon(\text{Mn I} - \text{Mn II}) &= -0.21 \text{ dex}, \\ \Delta \log \varepsilon(\text{Co I} - \text{Co II}) &= -0.16 \text{ dex}, \\ \Delta \log \varepsilon(\text{Ni I} - \text{Ni II}) &= -0.39 \text{ dex}. \end{aligned}$$

This can be understood as follows. Similar to Fe I, the listed neutrals are the minority species in the atmosphere of HE 2252–4225, and they are expected to be subject to ultra-violet overionisation resulting in weakened spectral lines compared with their LTE strengths, while the departures from LTE should be minor for the first ions, which are the majority species. For titanium, the difference in LTE abundances is largely removed, when applying the NLTE abundance corrections of 0.31 dex and 0.01 dex for Ti I and Ti II, respectively, as computed by Bergemann (2011) for the stellar parameters, $T_{\text{eff}} = 4600$ K, $\log g = 1.6$, and $[\text{Fe}/\text{H}] = -2.5$, close to those of HE 2252–4225. We note that the calculated NLTE effects for Ti I–II and Fe I–II are similar. In this study, we obtained $\Delta_{\text{NLTE}} = 0.26$ dex for Fe I and 0.00 for Fe II. However, significantly larger NLTE corrections of 0.44 dex and 0.64 dex were computed for Mn I (Bergemann & Gehren 2008) and Co I (Bergemann et al. 2010), respectively, using the same model, 4600/1.6/–2.5. Applying these corrections would lead to NLTE abundances that are too high for lines of neutral Mn and Co in HE 2252–4225 compared with those for their first ions. Here, we took into consideration that $\Delta_{\text{NLTE}} = 0.07$ dex for Co II (Bergemann et al. 2010) and assumed that $\Delta_{\text{NLTE}} < 0.1$ dex for Mn II. For Cr I–II, the NLTE calculations were performed for the MP dwarf stars (Bergemann & Cescutti 2010), but not giants. In the $[\text{Fe}/\text{H}] \approx -2.5$ stars, Δ_{NLTE} is of up to 0.35 dex for Cr I and 0.08 dex for Cr II. Larger positive corrections are required for the Cr I lines to remove abundance discrepancy between Cr I and Cr II in HE 2252–4225.

For Zn I 4810 Å in HE 2252–4225, the NLTE correction is expected to be small with $\Delta_{\text{NLTE}} = -0.02$ dex (Takeda et al.

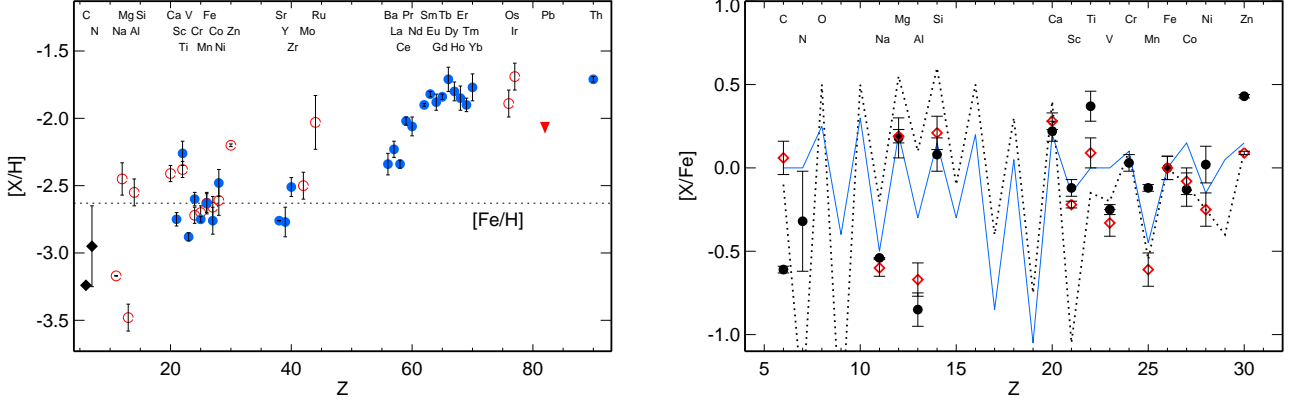


Fig. 3. Left panel: the element abundance pattern of HE 2252–4225. The filled rhombi, open circles, and filled circles display abundances derived from lines of molecules, neutral species, and singly ionised species, respectively. An upper limit for the Pb abundance is indicated by downward-facing triangle. The dotted line indicates the star’s iron abundance $[\text{Fe}/\text{H}] = -2.63$. Right panel: abundance patterns of HE 2252–4225 (filled circles) and HE 2327–5642 (open rhombi) in the C–Zn range compared with the yields of single supernova of $14.4 M_{\odot}$ (continuous line) as given by Lai et al. (2008) and the chemical evolution predictions of Kobayashi et al. (2011, dotted line). The first model provides $[(\text{C}+\text{N})/\text{Fe}]$. The corresponding value was plotted for HE 2327–5642, but not HE 2252–4225, where the uncertainty in derived N abundance is large.

2005). We assume that the departures from LTE for the second zinc line, $\text{Zn I } 4722 \text{ \AA}$, are as small, as is the case for $\text{Zn I } 4810 \text{ \AA}$. The NLTE effects for the heavy elements beyond the Fe group are discussed in Sect. 4.3.

In this study, we did not consider the influence of the 3D effects on the derived element abundances, although we took care to minimise such an influence, where possible, for example by removing low-excitation lines of Fe I and Mn I. Using the 3D hydrodynamic model atmosphere of VMP cool giant 5020/2.5–3, Dobrovolskas et al. (2013) predicted that the (3D–1D) abundance corrections are negative and large in absolute value of up to -0.6 to -0.75 dex for the lines arising from the ground state of the minority species, such as Mg I, Ti I, and Ni I, but they decrease rapidly towards higher excitation energy of the lower level and do not exceed -0.2 dex, when $E_{\text{exc}} = 2 \text{ eV}$. We did not determine such a large discrepancy between the $E_{\text{exc}} < 0.2$ and $E_{\text{exc}} > 2 \text{ eV}$ lines for Mg I and Ni I (Table 3, online material). In contrast to the predictions, the measured difference in 1D–LTE abundances ($\text{Ti I} - \text{Ti II}$) is negative, but not positive, and it is fully removed, when applying the 1D–NLTE abundance corrections. These results may cast a shadow of doubt on 3D calculations. However, our interpretation is that one cannot simply add 1D–NLTE and 3D–LTE results when both NLTE and 3D effects are significant. This is exactly the case in HE 2252–4225.

The heavy elements beyond the Fe group are mostly observed in HE 2252–4225 for their majority species, such as Ba II and Eu II, and in the low-excitation lines. Dobrovolskas et al. (2013) predicted that the (3D–1D) corrections for the $E_{\text{exc}} = 0$ lines of Ba II and Eu II are small and very similar in magnitude, -0.05 dex and -0.04 dex, respectively.

We comment below on abundances of individual groups of elements. The sample of cool giants from Cayrel et al. (2004, hereafter, Cayrel2004) was chosen as our comparison sample.

4.2. Lithium to zinc

Lithium. As expected for a red giant, HE 2252–4225 has a very low abundance of Li. The central depth of the Li I 6708 Å line

is about 1 % in the $S/N \approx 100$ observed spectrum, and only an upper limit of $\log \varepsilon_{\text{Li}} = -0.1$ was estimated.

Carbon and nitrogen. The C abundances obtained from CH lines in the regions 4310–4314 Å and 4362–4367 Å are consistent with each other to within 0.03 dex (see Table 3, online material). The mean abundance is $[\text{C}/\text{Fe}] = -0.61$, which is similar to those of the giants with $T_{\text{eff}} < 4800 \text{ K}$ from the sample of Cayrel2004. Such a low $[\text{C}/\text{Fe}]$ ratio in the cool giants is likely due to mixing, which has brought processed material to the surface from deep layers, where C is converted into N. This explains a factor of 2 higher N/C ratio in HE 2252–4225 compared with the solar value. The abundance of nitrogen could only be determined from the NH line at 3416.64 Å. We checked the spectral region around 3416.64 Å in the solar spectrum (Kurucz et al. 1984) and fitted it with gf -value of the NH line that had been reduced by -0.4 dex compared with what was calculated by Kurucz (1993). With this correction, we derived the relative abundance $[\text{N}/\text{Fe}] = -0.32$. It is worth noting that several papers applied “solar oscillator strengths” of the NH molecular lines, where Kurucz (1993) $\log gf$ -values were reduced by a factor of 0.807 dex (Hill et al. 2002), 0.4 dex (Aoki et al. 2006, Hayek et al. 2009, Mashonkina et al. 2010), and 0.3 dex (Shavrina et al. 1996, Johnson et al. 2007).

The α -process elements Mg, Si, Ca, and Ti are enhanced relative to iron: $[\text{Mg}/\text{Fe}] = 0.18$, $[\text{Si}/\text{Fe}] = 0.08$, $[\text{Ca}/\text{Fe}] = 0.22$, and $[\text{Ti}/\text{Fe}] = 0.37$ (from Ti II lines). This is in line with the behaviour of other metal-poor halo stars, although the $[\text{Mg}/\text{Fe}]$ and $[\text{Ca}/\text{Fe}]$ abundance ratios of HE 2252–4225 are significantly lower than $[\text{Mg}/\text{Fe}] = 0.61$ and $[\text{Ca}/\text{Fe}] = 0.50$ obtained by Andrievsky et al. (2010) and Spite et al. (2012) for the Cayrel2004 stellar sample when taking departures from LTE for Mg I and Ca I into account. The reason, most probably, is the use of different methods for determining surface gravity and iron abundance in Cayrel et al. (2004) and this paper. This is illustrated well by the results for HD 122563, which was included in the Cayrel2004 sample and which was also investigated in our earlier papers (Mashonkina et al. 2008, 2011) applying the same methods as in this study. The absolute NLTE abundances of HD 122563 for magnesium, $\log \varepsilon_{\text{Mg}} = 5.36$, and cal-

cium, $\log \varepsilon_{\text{Ca}} = 4.04$, as determined by Mashonkina et al. (2008), are similar to $\log \varepsilon_{\text{Mg}} = 5.39$ from Andrievsky et al. (2010) and $\log \varepsilon_{\text{Ca}} = 3.97$ from Spite et al. (2012). However, very different iron abundances of HD 122563 were determined in different studies. With $T_{\text{eff}} = 4600$ K, Cayrel et al. (2004) derived $\log g = 1.1$ and $[\text{Fe}/\text{H}] = -2.82$ from LTE analysis of Fe I and Fe II lines, while Mashonkina et al. (2008) calculated $\log g = 1.50$ from the HIPPARCOS parallax of HD 122563 and $[\text{Fe}/\text{H}] = -2.53$ from LTE analysis of Fe II lines. Mashonkina et al. (2011) have shown that NLTE leads to consistent iron abundances for the two ionisation stages, with $[\text{Fe}/\text{H}] = -2.56$, when employing $\log g = 1.60$ based on the updated HIPPARCOS parallax of HD 122563. It is worth noting that all three VMP giants with NLTE based gravity, metallicity, and element abundances available, i.e. HD 122563 (Mashonkina et al. 2008), HE 2327–5642 (Mashonkina et al. 2010), and HE 2252–4225 (this study) reveal moderate α -enhancement with $[\text{Mg}/\text{Fe}] = 0.18$ to 0.31 and $[\text{Ca}/\text{Fe}] = 0.21$ to 0.28 .

Sodium and aluminium. HE 2252–4225 displays an underabundance of the odd- Z elements Na and Al relative to iron of $[\text{Na}/\text{Fe}] = -0.54$ and $[\text{Al}/\text{Fe}] = -0.85$, and also relative to the even- Z element Mg of $[\text{Na}/\text{Mg}] = -0.72$ and $[\text{Al}/\text{Mg}] = -1.03$. This is not exceptional for a metal-poor halo star. From a NLTE analysis of the dwarf and giant stars in the range $-3.6 < [\text{Fe}/\text{H}] < -2.5$, Andrievsky et al. (2010) determined the mean values $[\text{Na}/\text{Mg}] \simeq -0.8$ and $[\text{Al}/\text{Mg}] \simeq -0.7$. The reason for the lower $[\text{Al}/\text{Mg}]$ ratio of HE 2252–4225 compared with that of the VMP stellar sample is, probably, the smaller positive NLTE correction computed in this study for the Al I line. For example, Fig. 2 from Andrievsky et al. (2008) displays $\Delta_{\text{NLTE}}(\text{Al I } 3961 \text{ \AA}) = 0.45$ dex for $T_{\text{eff}} = 4700$ K, $\log g = 1.65$, and $[\text{Fe}/\text{H}] = -2.5$, while we compute $\Delta_{\text{NLTE}}(\text{Al I } 3961 \text{ \AA}) = 0.14$ dex for the 4710/1.65/–2.66 model.

We could not make the source(s) of the discrepancy clear. Andrievsky et al. (2008) employed a modified version of the code MULTI (Carlsson 1986). We would not like to cast any shadow of doubt on the modification made by Korotin et al. (1999). Extensive tests of Bergemann et al. (2012) for Fe I–Fe II demonstrate very similar behaviour of departure coefficients computed with the codes MULTI (Carlsson 1986) and DETAIL (Butler & Giddings 1985), when using common input data. Bergemann et al. (2012) noted: “Perhaps, the only systematic effect is that MULTI predicts slightly stronger NLTE effects than DETAIL mainly due to the differences in the background opacity.” We performed test calculations for Al I with the code DETAIL by excluding the two sources from the background opacity, namely the lines of calcium and iron and quasi-molecular hydrogen absorption as described by Doyle (1968), and found larger departures from LTE compared with that for the standard opacity package (Fig. 4) and larger NLTE correction of $\Delta_{\text{NLTE}} = 0.33$ dex for Al I 3961 Å.

Scandium to nickel and zinc. Abundances of the elements in the nuclear charge range between $Z = 21$ and 28 were reliably determined from lines of either two ionisation stages or the majority species of a given element. As in Paper V, we did not use the Mn I resonance lines to calculate the mean presented in Table 5. In HE 2252–4225, the abundance difference between Mn I 4033 Å and the three Mn I subordinate lines amounts to -0.36 dex. It is worth noting that for each element X observed in HE 2252–4225 for two ionisation stages, the relative LTE abundances $[\text{X I}/\text{Fe I}]$ and $[\text{X II}/\text{Fe II}]$ are consistent with each other to within the error bars. We found that HE 2252–4225 is slightly deficient in the odd- Z elements Sc, V, Mn, and Co rel-

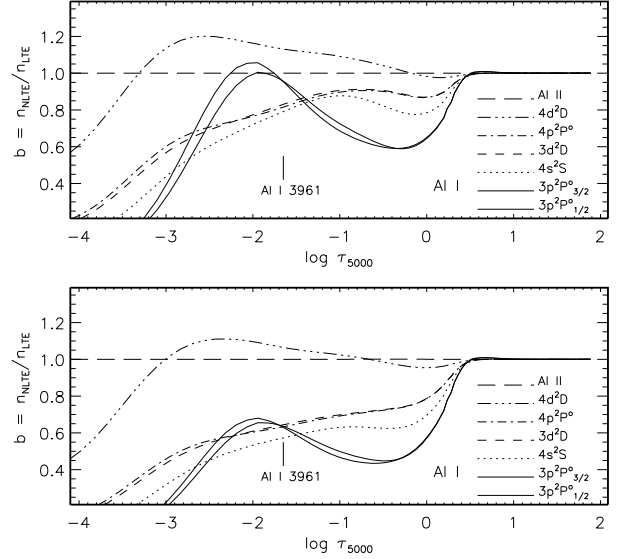


Fig. 4. Departure coefficients for selected levels of Al I as a function of $\log \tau_{5000}$ in the model atmosphere 4710/1.65/–2.66 from the calculations with the standard DETAIL opacity package (top panel) and with no lines of Fe and Ca and no quasi-molecular hydrogen absorption (bottom panel). Ticks indicate the locations of line-centre optical depth unity for the Al I line 3961 Å (transition $3p^2P_{3/2} - 4s^2S_{1/2}$).

ative to iron and solar ratios with very similar $[\text{Sc}/\text{Fe}]$, $[\text{Mn}/\text{Fe}]$, and $[\text{Co}/\text{Fe}]$ abundance ratios of -0.12 , -0.12 , and -0.13 , respectively, and $[\text{V}/\text{Fe}] = -0.25$. The abundance of Cr and, most probably, Ni follows the iron one. From the only line of Ni II at 3769.46 Å, we obtained $[\text{Ni II}/\text{Fe II}] = 0.15$, using the predicted gf -value from Kurucz (2003). The six lines of Ni I led to a close-to-solar ratio of $[\text{Ni I}/\text{Fe I}] = 0.02$. The investigated star is overabundant in Zn relative to iron with $[\text{Zn}/\text{Fe}] = 0.43$.

Lines of the first ions V II, Cr II, and Mn II were employed by Lai et al. (2008, hereafter, Lai2008) to derive the element abundances of the sample of 28 VMP stars. In the $-3.5 < [\text{Fe}/\text{H}] < -2.5$ range, they obtained, on average, close-to-solar ratios for $[\text{V II}/\text{Fe}]$ and $[\text{Cr II}/\text{Fe}]$ and a decline in $[\text{Mn II}/\text{Fe}]$ towards lower metallicity with $[\text{Mn II}/\text{Fe}] \simeq -0.2$ at $[\text{Fe}/\text{H}] \simeq -2.7$. Compared with the Lai2008 and Cayrel2004 stellar samples, HE 2252–4225 reveals similar element-to-iron abundance ratios for Cr, Mn, Ni, and Zn. However, HE 2252–4225 is slightly deficient in Sc, V, and Co relative to Fe, in contrast to stars of close metallicities in both VMP stellar samples.

We found that the element abundance pattern of HE 2252–4225 in the Na–Zn range (Fig. 3) resembles that of the VMP giant HE 2327–5642 (5050/2.34/–2.78), which was investigated in Paper V using the same methods as in this study. The star HE 2252–4225 has a significantly lower C abundance, presumably because it is a more evolved star compared with HE 2327–5642. The difference concerns with Ti, Mn, and Zn, which have higher abundances relative to Fe in HE 2252–4225 compared with HE 2327–5642.

On the basis of their Na to Zn abundances, HE 2252–4225 and HE 2327–5642 do not appear to be exceptional. Lai et al. (2008) fitted the average abundance pattern of their stellar sample to the entire library of single supernova (SN) yields, attempting to define a “typical” Population III star that has enriched the interstellar medium out of which the VMP stars formed. A fairly

good fit was obtained for SN of $14.4 M_{\odot}$. In Fig. 3, we compare the abundance patterns of HE 2252–4225 and HE 2327–5642 with the best fit model from Lai et al. (2008) and also the chemical evolution calculations of Kobayashi et al. (2011). In general, the single SN model fits the observations well. The exceptions are Al, V, and Co, which are overproduced in the model, and Ti, which, in contrast, is underproduced. The observed underabundances of V and Co relative to Fe are reproduced well by the model of Kobayashi et al. (2011).

4.3. Heavy elements: Sr to Th

We measured five light trans-iron elements with $38 \leq Z \leq 44$, 14 elements in the region of the second *r*-process peak, osmium and iridium, which represent the third peak, and the actinide thorium. For the Pb abundance, we could only estimate an upper limit.

Mashonkina & Christlieb (2014) showed an advantage of applying the NLTE approach when constraining a pure *r*-process Ba/Eu ratio from observations of the strongly *r*-process enhanced VMP stars. In this study, NLTE abundances were determined for five heavy elements: Sr, Ba, Eu, Pb, and Th. They are presented in Tables 5 and 3 (online material). The largest departures from LTE were found for Pb I 4057 Å. This can be understood, because Pb I represents a minor fraction of the element abundance, and its number density can easily deviate from the population in thermodynamic equilibrium, because of deviations in the mean intensity of ionising radiation from the Planck function. NLTE leads to overionisation of Pb I resulting in the weakened line and positive Δ_{NLTE} of 0.41 dex. Different NLTE mechanisms connected with the radiative bound-bound transitions are in action for Sr II, Ba II, Eu II, and Th II that represent a major fraction of their element abundances. The Sr II resonance lines are strong, and they are weakly affected by departures from LTE. The barium abundance of HE 2252–4225 was determined from the three subordinate lines, Ba II 5853, 6141, and 6497 Å, which are almost free of HFS effects. Our NLTE calculations for HE 2252–4225 showed that they are stronger than in the LTE case, resulting in a negative NLTE abundance correction of different magnitude for different lines, $\Delta_{\text{NLTE}} = -0.02$ dex, -0.17 dex, and -0.23 dex, respectively. NLTE largely removes the difference in LTE abundances between different Ba II lines, and the statistical error reduces to $\sigma_{\log \varepsilon} = 0.04$ dex. We calculated positive NLTE abundance corrections for the lines of Eu II and Th II, finding values close to $+0.1$ dex. All the elements from lanthanum to ytterbium are observed in the lines of their majority species, with term structures as complicated as that for Eu II and Th II, so the departures from LTE are expected to be similar to those for Eu II and Th II. This is largely true also for osmium and iridium detected in the lines of their neutrals, Os I and Ir I, which have relatively high ionisation energies of 8.44 and 8.97 eV, respectively. Fortunately, the abundance *ratios* among heavy elements except Ba are probably only weakly affected by departures from LTE. Indeed, the differences in mean abundance between Th and Eu are very similar in LTE and NLTE, -0.33 dex and -0.35 dex, respectively. For consistency, we used the abundances of the heavy elements beyond strontium as determined based on the LTE assumption.

The abundance analysis was based on line profile fitting. Figures 5 and 6 illustrate the quality of the fits for a few selected lines. For most chemical species, 2 to 19 spectral lines were employed, and nowhere does $\sigma_{\log \varepsilon}$ exceed 0.11 dex. For Mo, Ru, Yb, and Os, the abundance was derived from a single line. Mo I 3864 Å, Yb II 3694 Å, and Os I 4260 Å (Fig. 5, bottom

Table 6. Line list adopted for the spectrum synthesis of the 4019 Å blend.

Species	$\lambda(\text{\AA})$	$E_{\text{exc}}(\text{eV})$	$\log gf$	Refs.
Ce II	4018.820	1.546	−0.960	1
Nd II	4018.820	0.064	−0.880	1
Fe I	4018.887	4.256	−2.604	1
Ce II	4018.900	1.013	−1.220	1
Ce II	4018.927	0.635	−1.680	1
V I	4018.929	2.581	−0.557	1
¹³ CH	4018.956	0.463	−1.379	2
Pr II	4018.963	0.204	−1.030	1
Mn I	4018.987	4.354	−1.884	1
Fe I	4019.003	4.320	−1.793	1
¹³ CH	4019.010	0.463	−1.354	2
Fe I	4019.042	2.608	−2.780	1
V II	4019.044	3.753	−1.232	1
Ce II	4019.057	1.014	−0.530	1
Mn I	4019.066	4.666	−0.523	1
Ni I	4019.067	1.935	−3.121	1
Co I	4019.110	2.280	−3.287	3
Co I	4019.118	2.280	−3.173	3
Co I	4019.120	2.280	−3.876	3
Co I	4019.125	2.280	−3.298	3
Co I	4019.125	2.280	−3.492	3
Th II	4019.129	0.000	−0.228	1
Co I	4019.134	2.280	−3.287	3
V I	4019.134	1.804	−2.234	1
Co I	4019.135	2.280	−3.474	3
Co I	4019.138	2.280	−3.173	3
Co I	4019.140	2.280	−3.298	3
Ce II	4019.271	0.328	−2.320	1
Co I	4019.292	0.580	−4.371	1
Co I	4019.297	0.630	−3.432	1

Refs. 1 = VALD, 2 = Hill et al. (2002),
3 = Johnson & Bolte (2001).

right panel) were found to be free of blends in the spectrum of HE 2252–4225. Because of the high $S/N \approx 100$ of the observed spectrum in the relevant wavelength range, the uncertainty in the derived abundances was estimated as 0.1 dex. The observed feature at 3728.0–3728.2 Å (Fig. 5, top left panel) is attributed to a combination of the Ru I 3728.025 Å, Fe I 3728.044 Å, Nd II 3728.126 Å, and two lines of Ce II at 3728.019 and 3728.180 Å. For the blending lines, atomic data were taken from the VALD database (Kupka et al. 1999, hereafter, VALD). Ignoring the Ce II lines completely leads to a 0.1 dex higher ruthenium abundance. The uncertainty in Ru abundance grows, when considering a possible variation in the Nd and Fe abundances. We carefully estimate $\sigma_{\log \varepsilon} = 0.2$ dex for the Ru abundance obtained.

The radioactive element thorium was clearly detected in HE 2252–4225 in the two lines, Th II 4019 and 3741 Å (Fig. 6). To determine the Th abundance as accurately as possible, we updated the list of lines contributing to the 4019 Å blend. The used lines, together with the sources of atomic data, are indicated in Table 6. The second line, Th II 3741.183 Å, is located between the strong Ti I 3741.059 Å ($E_{\text{exc}}/\log gf = 0.02$ eV/−0.21) and Sm II 3741.276 Å (0.19 eV/−0.59) lines. Atomic data are indicated according to VALD. To fit the observed feature at 3741 Å in HE 2252–4225, we used a 0.6 dex lower *gf*-value of Ti I 3741 Å and $\log \varepsilon_{\text{Sm}} = -0.88$, which is only 0.02 dex higher than the obtained mean Sm abundance. The abundance derived from Th II 3741 Å agrees to within 0.03 dex with that for Th II 4019 Å.

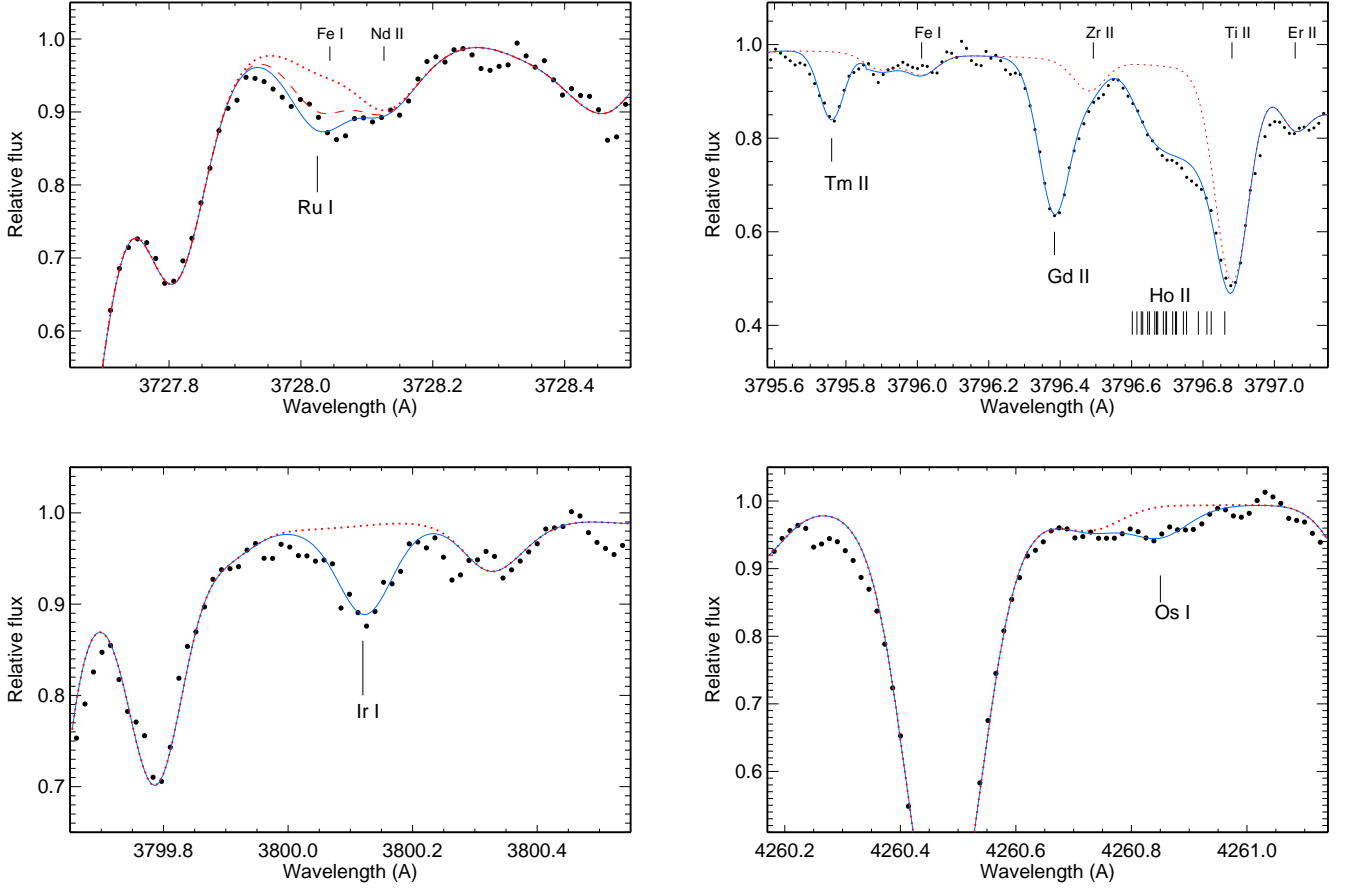


Fig. 5. Best fits (continuous curve) of the spectral ranges 3727.7–3728.5 Å and 3795.6–3797.1 Å (top row), where the investigated Ru I, Tm II, Gd II, and Ho II lines are located; Ir I 3800 Å and Os I 4260 Å (bottom row) in the observed spectrum of HE 2252–4225 (bold dots). The dotted curves show the synthetic spectrum with no relevant element in the atmosphere. The dashed curve in the top-left panel shows the effect of a 0.2 dex lower Ru abundance on the synthetic spectrum.

We attempted to detect the second actinide uranium. The only useful line, U II 3859.57 Å, lies between the two strong lines, Fe I 3859.21 Å and Fe I 3859.91 Å, in their overlapping wings. Our calculations with $[U/Fe] = 1$ predicted a depression of about 1 % at the U II 3859 Å line centre, however, no absorption feature was found at this place in the observed spectrum of HE 2252–4225. This indicates $[U/Fe] < 1$ for HE 2252–4225, although $[U/Fe] \approx 1$ cannot be ruled out, because the S/N is about 100 in this region.

It would be of great interest to know the Pb abundance of HE 2252–4225, since Th and U decay to the stable element lead. In the visual spectra, lead can only be observed in the two lines of similar strength, i.e. Pb I 3683 Å ($E_{\text{exc}} = 0.97$ eV, $\log gf = -0.52$) and 4057 Å ($E_{\text{exc}} = 1.32$ eV, $\log gf = -0.17$). However, the first line lies in a rather crowded spectral region, and most stellar Pb abundance analyses rely on using Pb I 4057 Å. In the spectrum of HE 2252–4225, there is a hint of a weak absorption feature at the Pb I 4057 Å line centre (Fig. 7). However, the S/N is quite low (≈ 80), and we could only estimate an upper limit for the Pb abundance to be $\log \varepsilon_{\text{LTE}} = -0.78$ and $\log \varepsilon_{\text{NLTE}} = -0.37$.

5. Heavy-element abundance pattern of HE 2252–4225 and r-II stars

This study confirms that HE 2252–4225 is enhanced in the heavy elements beyond Ba relative to iron and solar ratios (Fig. 3). For seven elements (i.e. Eu, Gd, Tb, Dy, Ho, Er, and Tm), where there is an r -process contribution to the SS matter of more than 80 % according to the predictions of Bisterzo et al. (2014, hereafter, Bisterzo2014), the average abundance ratio is $[r/Fe] = 0.80 \pm 0.06$. The obtained $[Ba/Eu] = -0.52$ is consistent with the earlier estimate $[Ba/Eu] = -0.54$ from Paper II, and the difference between $[Eu/Fe] = 0.81$ (this study) and $[Eu/Fe] = 0.99$ (Paper II) is mostly due to the higher revised iron abundance.

For the abundance comparison, we choose the four r-II stars with the largest number of measured species in the Sr–Th region. These are CS 22892-052 (Snedden et al. 2003), CS 31082-001 (Siqueira Mello et al. 2013), HE 1523-091 (Snedden et al. 2008), and HE 1219-0312 (Hayek et al. 2009). For each of them, the heavy-element abundances have been scaled to match Eu–Tm in HE 2252–4225, and the scaled abundances have been averaged. The average abundances are plotted in Fig. 8. The dispersion in the single star measurements around the mean does not exceed 0.1 dex for every investigated species except Th, indicating very similar abundance patterns of the r-II stars in the Sr–Ir region and a common origin of the first, second, and

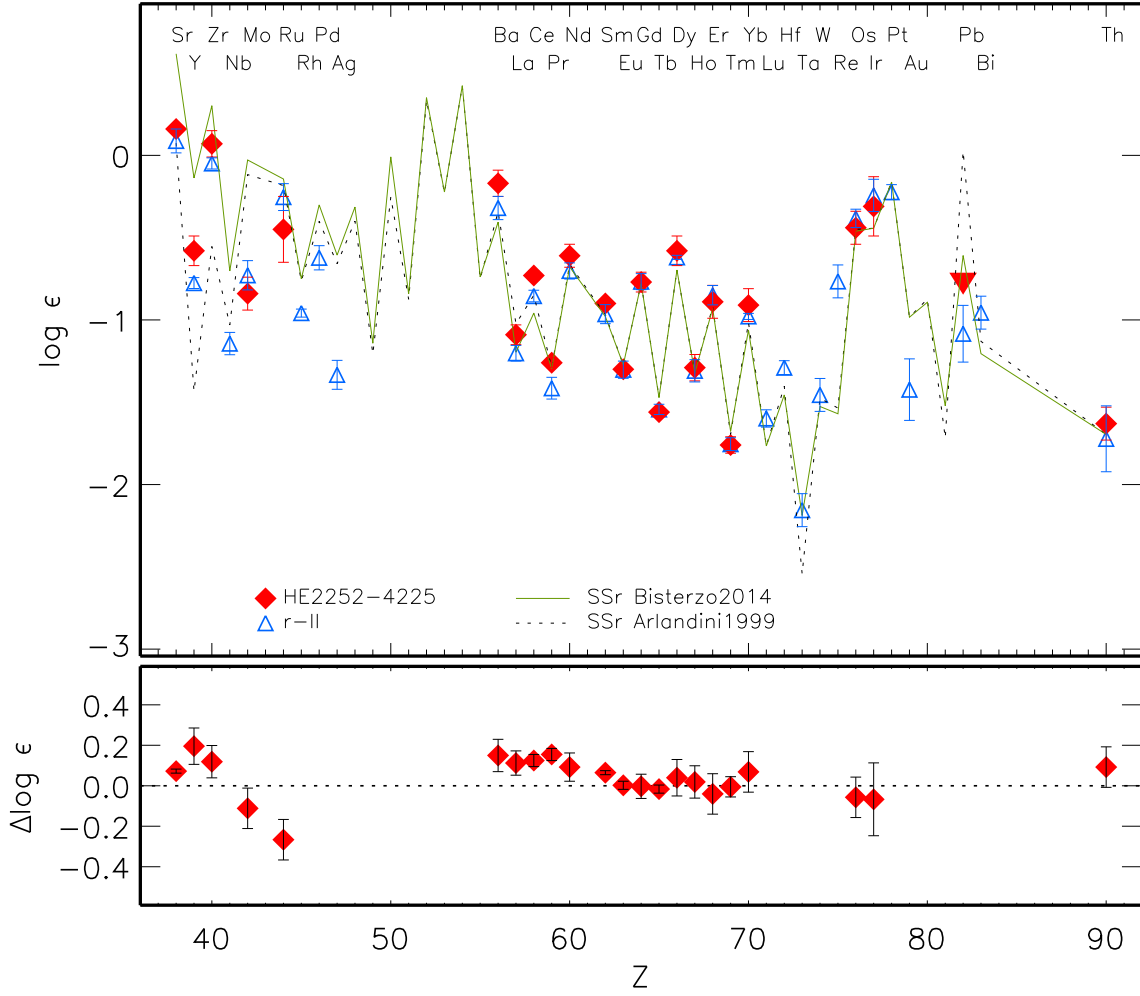


Fig. 8. Heavy-element abundance pattern of HE 2252–4225 (filled rhombi) compared with the average element abundances (open triangles) of the four benchmark r-II stars, CS 22892-052, CS 31082-001, HE 1523-0901, and HE 1219-0312. An upper limit for the Pb abundance of HE 2252–4225 is indicated by downward-facing triangle. For the r-II stars, the error bars show the dispersion in the single star measurements around the mean, when the species was measured in more than one star. Otherwise it was adopted as 0.1 dex. For comparison, the SSr abundance patterns calculated using the *s*-process predictions of Arlandini et al. (1999) (dotted curve) and Bisterzo et al. (2014) (continuous curve) are shown. They and also the heavy-element abundances of the r-II stars have been scaled to match Eu–Tm in HE 2252–4225. The bottom panel displays the difference between HE 2252–4225 and the r-II stars defined as $\Delta \log \epsilon = \log \epsilon_{\text{HE 2252-4225}} - \log \epsilon_{\text{r-II}}$.

third *r*-process peak elements in the classical *r*-process. It is clear from Fig. 8 that the elements in the range from Ba to Yb and also Os and Ir in HE 2252–4225 match the scaled abundances of the r-II stars very well, with a mean difference of $\Delta \log \epsilon = \log \epsilon_{\text{HE 2252-4225}} - \log \epsilon_{\text{r-II}} = 0.04 \pm 0.07$. No notable discrepancies between HE 2252–4225 and the r-II stars are also found for the light trans-iron elements Sr, Y, Zr, and Mo. For example $[\text{Sr}/\text{Eu}] = -0.94$ and $[\text{Zr}/\text{Eu}] = -0.69$ of HE 2252–4225 are in excellent agreement with the average abundance ratios $[\text{Sr}/\text{Eu}] = -0.92 \pm 0.13$ and $[\text{Zr}/\text{Eu}] = -0.64 \pm 0.19$ calculated in Paper V for nine r-II stars, and they are significantly lower than the corresponding values, -0.56 and -0.31 , for the 32 r-I stars. Thus, HE 2252–4225 should be referred to as r-II star, despite the slightly low derived europium enhancement of $[\text{Eu}/\text{Fe}] = 0.81$ (LTE) and 0.91 (NLTE).

As proposed by Mashonkina et al. (2010), a membership of a given *r*-process enhanced MP star to the r-II or r-I group could be connected to an origin of the neutron-capture elements, if a separation involved the criteria based on not only $[\text{Eu}/\text{Fe}]$ and $[\text{Ba}/\text{Eu}]$, but also $[\text{Sr}/\text{Eu}]$. For example, the well-studied stars

HD 221170 (Ivans et al. 2006) and BD +17°3248 (Cowan et al. 2002) have very similar $[\text{Eu}/\text{Fe}] = 0.80$ and 0.91 and $[\text{Ba}/\text{Eu}] = -0.54$ and -0.51 to those for HE 2252–4225, and by definition (Paper I), all three objects are of type r-I. However, $[\text{Sr}/\text{Eu}]$ ratios of -0.67 and -0.62 for HD 221170 and BD +17°3248, respectively, are higher than for HE 2252–4225 (-0.94), and an origin of the first *r*-process peak elements in HD 221170 and BD +17°3248 remains unclear.

In Fig. 8, we also plot the scaled solar *r*-process residuals calculated by subtracting theoretical *s*-process yields from the observed SS total abundance. For the latter, we rely on the meteoritic abundances of Lodders et al. (2009). For the solar *s*-abundances, we consider the *s*-process predictions of Arlandini et al. (1999, stellar model; hereafter, Arlandini1999) and Bisterzo et al. (2014). Arlandini1999 used stellar AGB models of 1.5 and $3 M_{\odot}$ with half solar metallicity. Bisterzo2014 performed the Galactic chemical evolution (GCE) calculations that considered the *s*-process contributions from different generations of AGB stars of various mass. Hereafter, the solar *r*-residuals are referred to as the solar system *r*-process (SSr) abun-

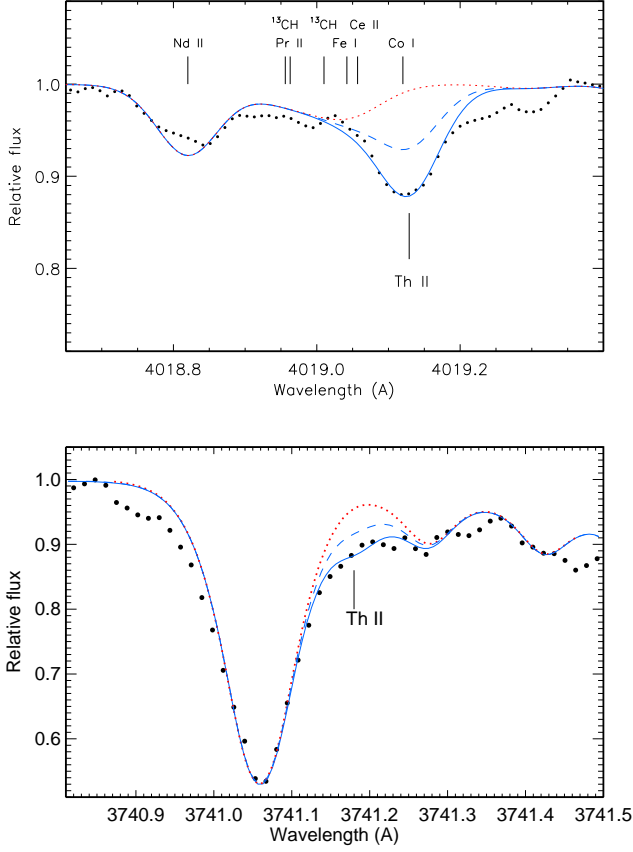


Fig. 6. Same as in Fig. 5 for Th II 4019 Å (top panel) and Th II 3741 Å (bottom panel). The dashed curves show the effect of a 0.3 dex lower Th abundance on the synthetic spectrum.

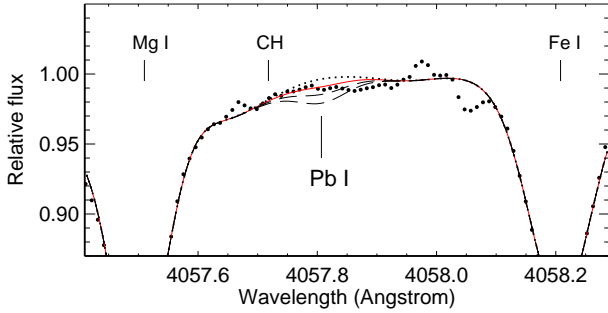


Fig. 7. $S/N \approx 80$ spectrum of HE 2252–4225 (bold dots) in the region, where the Pb I 4057 Å line is located. The synthetic spectra were computed with no Pb in the atmosphere (dotted curve), $\log \varepsilon_{\text{Pb}} = -0.78$ (continuous curve), -0.48 , and -0.28 (dashed curves for both values).

dance pattern. A notable difference between two sets of the solar *r*-residuals was obtained for all elements with dominant *s*-process contribution to their solar abundances. For example for Sr, Y, and Zr, Arlandini1999 predicted a main *s*-process contribution of 85, 92, and 83 %, respectively, while the corresponding numbers in Bisterzo2014 are 69, 72, and 66%.

The elements in the range from La to Yb and also the third *r*-process peak elements Os and Ir in HE 2252–4225 were found to match the solar *r*-process pattern very well, with a mean dif-

ference of $\Delta \log \varepsilon = \log \varepsilon_{\text{HE 2252–4225}} - \text{SSr} = 0.03 \pm 0.07$ and 0.05 ± 0.08 for the solar *r*-abundances of Arlandini1999 and Bisterzo2014, respectively. This finding is in line with the earlier results obtained for other *r*-process rich stars (for a review, see Sneden et al. 2008) and provides additional evidence of universal production ratio of these elements during the Galactic history. As for Ba, it does matter whether its stellar abundance and also abundances of the *r*-process elements are determined in LTE or NLTE. The difference between the barium LTE abundance of HE 2252–4225 and the scaled solar *r*-abundance amounts to 0.17 dex and 0.24 dex for the data of Arlandini1999 and Bisterzo2014, respectively. Our calculations show that NLTE leads to a 0.15 dex lower Ba, but 0.10 dex higher Eu abundance of HE 2252–4225 and, thus, removes the difference in Ba abundance between HE 2252–4225 and SSr of Bisterzo2014, when assuming the NLTE corrections for Gd–Tm abundances to be similar to those for Eu.

6. Thorium in *r*-process enhanced stars

It would be rather challenging to determine the stellar age of HE 2252–4225 by comparing the observed Th-to-stable neutron-capture element-abundance ratios with the corresponding initial values at the time when the star was born, $\log(\text{Th}/X)_0$:

$$\tau = 46.7 \text{ Gyr} [\log(\text{Th}/X)_0 - \log(\text{Th}/X)_{\text{obs}}].$$

For HE 2252–4225, the ratio $\log(\text{Th}/\text{Eu})_{\text{obs}} = -0.33$ (LTE) or -0.35 (NLTE) deviates by only a little, 0.01 or 0.03 dex, from the solar *r*-residual ratio $\log(\text{Th}/\text{Eu})_0 = -0.32$ (Bisterzo2014), resulting in too low an age of $\tau < 1.5$ Gyr. Since the Sun is approximately 4.5 Gyr old, a corresponding correction of +0.1 dex accounting for the thorium radioactive decay was introduced to the solar current thorium abundance. To be as old as the galactic halo VMP stars, HE 2252–4225 should have an approximately 0.3 dex lower Th abundance. Figure 6 displays the effect of a variation in Th abundance on the synthetic spectrum of Th II 4019 Å and Th II 3741 Å. It is evident that the stellar Th abundance cannot be significantly lower than $\log \varepsilon_{\text{Th}} = -1.63$. The observational error represented by the dispersion in the measurements of multiple lines around the mean amounts to $\sigma_{\log \varepsilon} = 0.02$ dex for Th/Eu of HE 2252–4225. The systematic errors linked to our choice of stellar parameters have a common sign and very similar magnitudes for lines of Eu II and Th II, i.e. 0.08 dex and 0.09 dex, respectively. Thus, the total uncertainty in Th/Eu is small, and it is translated to an uncertainty of less than 1.5 Gyr for the age of HE 2252–4225.

Application of the above formula to the Th/*X* pairs involving other *r*-process elements leads to $\tau = 1.9$ to 3.3 Gyr for Gd, Ho, Er, and Os, $\tau = 7.0$ and 7.9 Gyr for Dy and Ir, and negative age for Tb and Tm. It is clear that Th does appear to be enhanced in HE 2252–4225 to a higher level than observed for elements of the second and third *r*-process peaks, and HE 2252–4225 belongs to the group of the so-called actinide boost stars.

The first discovered star with an anomalously high Th/Eu abundance ratio of $\log(\text{Th}/\text{Eu}) = -0.22$ was CS 31082–001 (Hill et al. 2002). Roederer et al. (2009) revised Eu and Th abundances of 15 MP stars that reveal pure *r*-process neutron-capture elements. Figure 9 displays the Th/Eu abundance ratios of the Roederer et al. (2009) sample and also HE 2327–5642 (Paper V), CS 30315–029 (Siqueira-Mello et al. 2014), and HE 2252–4225. It appears that 12 of the 18 stars have no obvious enhancement of thorium with respect to the scaled solar *r*-process pattern, and for each of them, its stellar age agrees within the error bars with the cosmic age

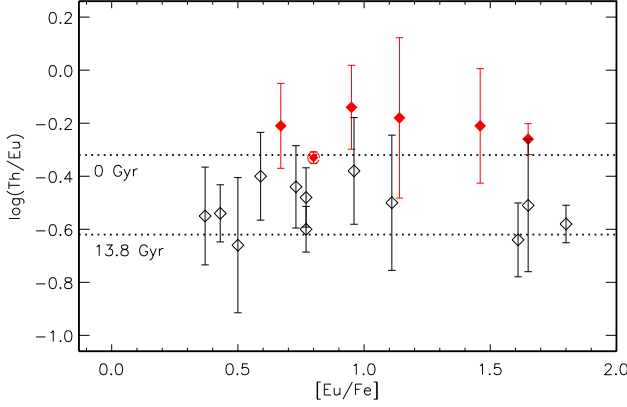


Fig. 9. Th/Eu abundance ratios of the Roederer et al. (2009) sample, HE 2327–5642 (Paper V), CS 30315–029 (Siqueira-Mello et al. 2014), and HE 2252–4225 (filled rhomb inside open circle). Stars with high Th/Eu ratios ($\log(\text{Th}/\text{Eu}) \geq -0.35$) are shown by filled rhombi and the remaining stars with open rhombi. The horizontal lines indicate the ratios expected if a sample of material had a given age, assuming the solar *r*-process of Bisterzo 2014.

13.772 ± 0.059 Gyr (Bennett et al. 2013) derived from the updated results of the *Wilkinson Microwave Anisotropy Probe* (WMAP). For example, $\tau = 14.9 \pm 6.5$ Gyr was calculated for CS 22892–052 with $\log(\text{Th}/\text{Eu}) = -0.64$. The remaining six stars, namely, CS 31082–001, CS 30306–132 (discovered by Honda et al. 2004), CS 31078–018 (Lai et al. 2008), HE 1219–0312 (Hayek et al. 2009), CS 30315–029 (Siqueira-Mello et al. 2014), and HE 2252–4225, exhibit an actinide boost, and their ages cannot be derived when only a single radioactive element Th is detected. Indeed, a negative age of $\tau = -4.7$ Gyr is calculated for CS 31082–001, when using the Th/Eu abundance ratio. This implies that thorium in the actinide boost stars was overproduced compared with the normal Th/Eu stars and the SS matter. Only the detection of the second actinide, uranium, made possible an estimation of the stellar age of CS 31082–001 through analysis of U/Th; i.e., $\tau = 12.5 \pm 3$ Gyr was first obtained by Cayrel et al. (2001), and the revised value is $\tau = 14.0 \pm 2.4$ Gyr (Hill et al. 2002). This provided solid evidence that different *r*-process nucleosynthesis events may produce significantly different yields in the actinide region ($Z \geq 90$). To find out whether variations in progenitor mass or explosion energy, or other intrinsic and environmental factors, or all of these, influence the *r*-process yields for the heaviest elements, more measurements of Th and U abundances in stars should be done.

7. Conclusions

We revised the stellar parameters and performed a detailed abundance analysis of the VMP giant HE 2252–4225 using high-quality VLT/UVES spectra and refined theoretical methods of line-formation modelling. The effective temperature, $T_{\text{eff}} = 4710$ K, previously derived in Paper II was confirmed through analysis of the $\text{H}\alpha$ and $\text{H}\beta$ line wings in HE 2252–4225. The surface gravity, $\log g = 1.65$, the iron abundance, $[\text{Fe}/\text{H}] = -2.63$, and the microturbulence velocity, $\xi_t = 1.7 \text{ km s}^{-1}$, were calculated from the NLTE ionisation balance between Fe I and Fe II.

Accurate abundances for a total of 38 elements from C to Th were determined in HE 2252–4225. For each chemical

species, the dispersion in the single line measurements around the mean does not exceed 0.12 dex. The investigated star was found to be deficient in carbon, as expected for a giant star with $T_{\text{eff}} < 4800$ K. The elements in the range from Na to Zn reveal a typical behaviour of the galactic halo VMP stars. The Na–Zn abundance pattern of HE 2252–4225 is well fitted by the yields of a single supernova of $14.4 M_{\odot}$, similar to the Lai et al. (2008) stellar sample.

We confirmed that HE 2252–4225 is *r*-process enhanced, having $[r/\text{Fe}] = 0.80 \pm 0.06$. The investigated star and four benchmark *r*-II stars; i.e., CS 22892–052 (Snedden et al. 2003), CS 31082–001 (Siqueira Mello et al. 2013), HE 1219–0312 (Hayek et al. 2009), and HE 1523–091 (Snedden et al. 2008) have very similar abundance patterns of the elements in the range from Sr to Ir. Hence, neutron-capture elements beyond Sr and up to Ir in HE 2252–4225 have a common origin in the classical main *r*-process. Applying the third criterion, $[\text{Sr}/\text{Eu}] < -0.8$ (Mashonkina et al. 2010), in addition to the two, $[\text{Eu}/\text{Fe}] > +1$ and $[\text{Ba}/\text{Eu}] < 0$, as suggested by Christlieb et al. (2004), makes membership to *r*-II stars have a physical sense related to an origin of the neutron-capture elements in the star; i.e., an *r*-II star can be defined as a star having neutron-capture elements originating in a single *r*-process.

We tested the solar *r*-process pattern based on recent *s*-process calculations of Bisterzo et al. (2014) and found that the elements in the range from Ba to Ir in HE 2252–4225 match it very well. No firm conclusion can be drawn about the relationship between the first neutron-capture peak elements, Sr to Ru, in HE 2252–4225 and the solar *r*-process, owing to the uncertainty in the solar *r*-process.

The star HE 2252–4225 has an anomalously high Th/Eu abundance ratio, so that radioactive age dating results in a stellar age of $\tau = 1.5 \pm 1.5$ Gyr that is not expected for a very metal-poor halo star. This is the sixth star in the group of actinide boost stars. Understanding the mechanisms resulting in different yields in the actinide region from different *r*-process events is a challenge for nucleosynthesis theory and requires studying larger samples of *r*-I and *r*-II stars.

Acknowledgements. This work was supported by Sonderforschungsbereich SFB 881 “The Milky Way System” (subprojects A4 and A5) of the German Research Foundation (DFG). L.M. is supported by the Russian Foundation for Basic Research (grant 14-02-91153) and the Swiss National Science Foundation (SCOPES project No. IZ73Z0-152485). We made use the NIST and VALD databases.

References

- Alexeeva, S., Pakhomov, Y., & Mashonkina, L. 2014, *Astronomy Letters*, 40, 406
- Andrievsky, S. M., Spite, M., Korotin, S. A., et al. 2010, *A&A*, 509, A88
- Andrievsky, S. M., Spite, M., Korotin, S. A., et al. 2008, *A&A*, 481, 481
- Anstee, S. D. & O’Mara, B. J. 1995, *MNRAS*, 276, 859
- Aoki, W., Beers, T. C., Honda, S., & Carollo, D. 2010, *ApJ*, 723, L201
- Aoki, W., Frebel, A., Christlieb, N., et al. 2006, *ApJ*, 639, 897
- Aoki, W., Honda, S., Beers, T. C., et al. 2005, *ApJ*, 632, 611
- Arlandini, C., Käppeler, F., Wisshak, K., et al. 1999, *ApJ*, 525, 886
- Bagnulo, S., Jehin, E., Ledoux, C., et al. 2003, *The Messenger*, 114, 10
- Bard, A., Kock, A., & Kock, M. 1991, *A&A*, 248, 315
- Barklem, P. S. & Aspelund-Johansson, J. 2005, *A&A*, 435, 373
- Barklem, P. S., Belyaev, A. K., Dickinson, A. S., & Gad  a, F. X. 2010, *A&A*, 519, A20
- Barklem, P. S., Belyaev, A. K., Spielfiedel, A., Guitou, M., & Feautrier, N. 2012, *A&A*, 541, A80
- Barklem, P. S., Christlieb, N., Beers, T. C., et al. 2005, *A&A*, 439, 129, (Paper II)
- Barklem, P. S. & O’Mara, B. J. 1997, *MNRAS*, 290, 102
- Barklem, P. S. & O’Mara, B. J. 1998, *MNRAS*, 300, 863
- Barklem, P. S., O’Mara, B. J., & Ross, J. E. 1998, *MNRAS*, 296, 1057

- Barklem, P. S., Piskunov, N., & O'Mara, B. J. 2000, *A&A*, 363, 1091
- Baummueller, D. & Gehren, T. 1996, *A&A*, 307, 961
- Beers, T., Flynn, C., Rossi, S., et al. 2007, *ApJ Suppl.*, 168, 128
- Belyakova, E. V. & Mashonkina, L. I. 1997, *Astronomy Reports*, 41, 530
- Bennett, C. L., Larson, D., Weiland, J. L., et al. 2013, *ApJS*, 208, 20
- Bergemann, M. 2011, *MNRAS*, 413, 2184
- Bergemann, M. & Cescutti, G. 2010, *A&A*, 522, A9
- Bergemann, M. & Gehren, T. 2008, *A&A*, 492, 823
- Bergemann, M., Lind, K., Collet, R., Magic, Z., & Asplund, M. 2012, *MNRAS*, 427, 27
- Bergemann, M., Pickering, J. C., & Gehren, T. 2010, *MNRAS*, 401, 1334
- Biémont, E., Dutriex, J.-F., Martin, I., & Quinet, P. 1998, *Journal of Physics B Atomic Molecular Physics*, 31, 3321
- Biémont, E., Garnir, H. P., Palmeri, P., Li, Z. S., & Svanberg, S. 2000, *MNRAS*, 312, 116
- Biemont, E., Grevesse, N., Faires, L. M., et al. 1989, *A&A*, 209, 391
- Bisterzo, S., Travaglio, C., Gallino, R., Wiescher, M., & Käppeler, F. 2014, *ApJ*, 787, 10
- Blackwell, D. E., Ibbetson, P. A., Petford, A. D., & Shallis, M. J. 1979, *MNRAS*, 186, 633
- Blackwell, D. E., Petford, A. D., Shallis, M. J., & Simmons, G. J. 1982a, *MNRAS*, 199, 43
- Blackwell, D. E., Petford, A. D., & Simmons, G. J. 1982b, *MNRAS*, 201, 595
- Borghs, G., de Bisschop, P., van Hove, M., & Silverans, R. E. 1983, *Hyperfine Interactions*, 15, 177
- Butler, K. & Giddings, J. 1985, *Newsletter on the analysis of astronomical spectra*, No. 9, University of London
- Cardon, B. L., Smith, P. L., Scalo, J. M., Testerman, L., & Whaling, W. 1982, *ApJ*, 260, 395
- Carlsson, M. 1986, *Uppsala Astronomical Observatory Reports*, 33
- Cayrel, R., Depagne, E., Spite, M., et al. 2004, *A&A*, 416, 1117
- Cayrel, R., Hill, V., Beers, T. C., et al. 2001, *Nature*, 409, 691
- Chang, T. N. & Tang, X. 1990, *J. Quant. Spec. Radiat. Transf.*, 43, 207
- Christlieb, N., Beers, T. C., Barklem, P. S., et al. 2004, *A&A*, 428, 1027, (Paper I)
- Christlieb, N., Schörck, T., Frebel, A., et al. 2008, *A&A*, 484, 721
- Collet, R., Asplund, M., & Trampedach, R. 2007, *A&A*, 469, 687
- Cowan, J. J., Sneden, C., Beers, T. C., et al. 2005, *ApJ*, 627, 238
- Cowan, J. J., Sneden, C., Burles, S., et al. 2002, *ApJ*, 572, 861
- Cowley, C. R. & Corliss, C. H. 1983, *MNRAS*, 203, 651
- Creevey, O. L., Thévenin, F., Boyajian, T. S., et al. 2012, *A&A*, 545, A17
- Den Hartog, E. A., Lawler, J. E., Sneden, C., & Cowan, J. J. 2003, *Astrophys. J. Suppl. Ser.*, 148, 543
- Den Hartog, E. A., Lawler, J. E., Sneden, C., & Cowan, J. J. 2006, *Astrophys. J. Suppl. Ser.*, 167, 292
- Den Hartog, E. A., Lawler, J. E., Sobeck, J. S., Sneden, C., & Cowan, J. J. 2011, *ApJS*, 194, 35
- Dobrovolskas, V., Kučinskas, A., Steffen, M., et al. 2013, *A&A*, 559, A102
- Doyle, R. O. 1968, *ApJ*, 153, 987
- Drawin, H.-W. 1968, *Zeitschrift für Physik*, 211, 404
- Drawin, H. W. 1969, *Zeitschrift für Physik*, 225, 483
- François, P., Depagne, E., Hill, V., et al. 2007, *A&A*, 476, 935
- Frebel, A., Christlieb, N., Norris, J. E., et al. 2007, *ApJ*, 660, L117
- Fuhr, J. R., Martin, G. A., & Wiese, W. L. 1988, *Journal of Physical and Chemical Reference Data*, 17
- Fuhr, J. R. & Wiese, W. L. 1992, *NIST Atomic Transition Probability Tables, CRC Handbook of Chemistry & Physics, 77th Edition*, D. R. Lide (CRC Press, Inc., Boca Raton, FL)
- Ginibre, A. 1989, *Phys. Scr.*, 39, 694
- Gustafsson, B., Edvardsson, B., Eriksson, K., et al. 2008, *A&A*, 486, 951
- Hannaford, P., Lowe, R. M., Grevesse, N., Biémont, E., & Whaling, W. 1982, *ApJ*, 261, 736
- Hayek, W., Asplund, M., Collet, R., & Nordlund, Å. 2011, *A&A*, 529, A158
- Hayek, W., Wiesendahl, U., Christlieb, N., et al. 2009, *A&A*, 504, 511
- Hill, V., Plez, B., Cayrel, R., et al. 2002, *A&A*, 387, 560
- Holt, R. A., Scholl, T. J., & Rosner, S. D. 1999, *MNRAS*, 306, 107
- Honda, S., Aoki, W., Kajino, T., et al. 2004, *ApJ*, 607, 474
- Ivans, I. I., Simmerer, J., Sneden, C., et al. 2006, *ApJ*, 645, 613
- Ivarsson, S., Andersen, J., Nordström, B., et al. 2003, *Astron. and Astrophys.*, 409, 1141
- Ivarsson, S., Litzén, U., & Wahlgren, G. M. 2001, *Physica Scripta*, 64, 455
- Johnson, J. A. & Bolte, M. 2001, *ApJ*, 554, 888
- Johnson, J. A., Herwig, F., Beers, T. C., & Christlieb, N. 2007, *ApJ*, 658, 1203
- Kling, R. & Griesmann, U. 2000, *ApJ*, 531, 1173
- Kobayashi, C., Karakas, A. I., & Umeda, H. 2011, *MNRAS*, 414, 3231
- Korotin, S. A., Andrievsky, S. M., & Luck, R. E. 1999, *A&A*, 351, 168
- Kupka, F., Piskunov, N., Ryabchikova, T. A., Stempels, H. C., & Weiss, W. W. 1999, *A&AS*, 138, 119, (VALD)
- Kurucz, R. L. 1993, *SYNTHE Spectrum Synthesis Programs and Line Data. Kurucz CD-ROM No. 18*. Cambridge, Mass.: Smithsonian Astrophysical Observatory, 1993, 18.
- Kurucz, R. L. 1994, *Opacities for Stellar Atmospheres. CD-ROM No. 2-8* (Cambridge, Mass)
- Kurucz, R. L. 2003, Robert L. Kurucz on-line database of observed and predicted atomic transitions
- Kurucz, R. L. 2005, *Memorie della Societa Astronomica Italiana Supplementi*, 8, 14
- Kurucz, R. L., Furenlid, I., Brault, J., & Testerman, L. 1984, *Solar flux atlas from 296 to 1300 nm* (New Mexico: National Solar Observatory)
- Lai, D. K., Bolte, M., Johnson, J. A., et al. 2008, *ApJ*, 681, 1524
- Lawler, J. E., Bonvallet, G., & Sneden, C. 2001a, *ApJ*, 556, 452
- Lawler, J. E. & Dakin, J. T. 1989, *Journal of the Optical Society of America B Optical Physics*, 6, 1457
- Lawler, J. E., Den Hartog, E. A., Sneden, C., & Cowan, J. J. 2006, *Astrophys. J. Suppl. Ser.*, 162, 227
- Lawler, J. E., Guzman, A., Wood, M. P., Sneden, C., & Cowan, J. J. 2013, *ApJS*, 205, 11
- Lawler, J. E., Sneden, C., & Cowan, J. J. 2004, *ApJ*, 604, 850
- Lawler, J. E., Sneden, C., Cowan, J. J., Ivans, I. I., & Den Hartog, E. A. 2009, *Astrophys. J. Suppl. Ser.*, 182, 51
- Lawler, J. E., Sneden, C., Cowan, J. J., et al. 2008, *ApJS*, 178, 71
- Lawler, J. E., Wickliffe, M. E., Cowley, C. R., & Sneden, C. 2001b, *Astrophys. J. Suppl. Ser.*, 137, 341
- Lawler, J. E., Wickliffe, M. E., den Hartog, E. A., & Sneden, C. 2001c, *ApJ*, 563, 1075
- Lawler, J. E., Wyart, J.-F., & Blaise, J. 2001d, *ApJS*, 137, 351
- Lefebvre, P.-H., Garnir, H.-P., & Biémont, E. 2003, *A&A*, 404, 1153
- Ljung, G., Nilsson, H., Asplund, M., & Johansson, S. 2006, *A&A*, 456, 1181
- Lodders, K., Plame, H., & Gail, H.-P. 2009, in *Landolt-Börnstein - Group VI Astronomy and Astrophysics Numerical Data and Functional Relationships in Science and Technology Volume 4B: Solar System*. Edited by J.E. Trümper, 2009, 4.4., 44–54
- Mårtensson-Pendrill, A.-M., Gough, D. S., & Hannaford, P. 1994, *Phys. Rev. A*, 49, 3351
- Malcheva, G., Blagoev, K., Mayo, R., et al. 2006, *MNRAS*, 367, 754
- Mashonkina, L. 2013, *A&A*, 550, A28
- Mashonkina, L. & Christlieb, N. 2014, *A&A*, 565, A123
- Mashonkina, L., Christlieb, N., Barklem, P. S., et al. 2010, *A&A*, 516, A46, (Paper V)
- Mashonkina, L. & Gehren, T. 2000, *A&A*, 364, 249
- Mashonkina, L. & Gehren, T. 2001, *A&A*, 376, 232
- Mashonkina, L., Gehren, T., & Biskmaev, I. 1999, *A&A*, 343, 519
- Mashonkina, L., Gehren, T., Shi, J.-R., Korn, A. J., & Grupp, F. 2011, *A&A*, 528, A87
- Mashonkina, L., Korn, A. J., & Przybilla, N. 2007a, *A&A*, 461, 261
- Mashonkina, L., Ryabtsev, A., & Frebel, A. 2012, *A&A*, 540, A98
- Mashonkina, L., Zhao, G., Gehren, T., et al. 2008, *A&A*, 478, 529
- Mashonkina, L. I., Vinogradova, A. B., Ptitsyn, D. A., Khokhlova, V. S., & Chernetsova, T. A. 2007b, *Astronomy Reports*, 51, 903
- McWilliam, A., Preston, G. W., Sneden, C., & Searle, L. 1995, *AJ*, 109, 2757
- Meggers, W. F., Corliss, C. H., & Scribner, B. F. 1975, *Tables of spectral-line intensities. Part I, II- arranged by elements.*, ed. Meggers, W. F., Corliss, C. H., & Scribner, B. F.
- Meléndez, J. & Barbuy, B. 2009, *A&A*, 497, 611
- Nilsson, H., Ljung, G., Lundberg, H., & Nielsen, K. E. 2006, *Astron. and Astrophys.*, 445, 1165
- Nilsson, H., Zhang, Z. G., Lundberg, H., Johansson, S., & Nordström, B. 2002, *Astron. and Astrophys.*, 382, 368
- Nitz, D. E., Kunau, A. E., Wilson, K. L., & Lentz, L. R. 1999, *ApJS*, 122, 557
- O'brian, T. R. & Lawler, J. E. 1991, *Phys. Rev. A*, 44, 7134
- Pickering, J. C. 1996, *ApJS*, 107, 811
- Pickering, J. C., Thorne, A. P., & Perez, R. 2001, *ApJS*, 132, 403
- Pinnington, E. H., Ji, Q., Guo, B., et al. 1993, *Canadian Journal of Physics*, 71, 470
- Ralchenko, Y. A., Kramida, E., Reader, J., & Team, N. A. 2008, *NIST Atomic Spectra Database (version 3.1.5)* (USA)
- Reader, J., Corliss, C. H., Wiese, W. L., & Martin, G. A. 1980, *Wavelengths and transition probabilities for atoms and atomic ions: Part 1. Wavelengths, part 2. Transition probabilities*
- Reetz, J. K. 1991, *Diploma Thesis (Universität München)*
- Roederer, I. U., Kratz, K.-L., Frebel, A., et al. 2009, *ApJ*, 698, 1963
- Roederer, I. U. & Lawler, J. E. 2012, *ApJ*, 750, 76
- Salih, S., Lawler, J. E., & Whaling, W. 1985, *Phys. Rev. A*, 31, 744
- Sansonetti, C. J., Richou, B., Engleman, Jr., R., & Radziemski, L. J. 1995, *Phys. Rev. A*, 52, 2682
- Schlegel, D. J., Finkbeiner, D. P., & Davis, M. 1998, *ApJ*, 500, 525

- Shavrina, A. V., Yakovina, L. A., & Bikmaev, I. F. 1996, *Kinematics and Physics of Celestial Bodies*, 12, 35
- Shi, J. R., Gehren, T., Butler, K., Mashonkina, L. I., & Zhao, G. 2008, *A&A*, 486, 303
- Siqueira-Mello, C., Hill, V., Barbuy, B., et al. 2014, *ArXiv e-prints*
- Siqueira Mello, C., Spite, M., Barbuy, B., et al. 2013, *A&A*, 550, A122
- Sitnova, T. M. & Mashonkina, L. I. 2011, *Astronomy Letters*, 37, 480
- Smith, G. 1981, *A&A*, 103, 351
- Smith, G. & O’Neill, J. A. 1975, *A&A*, 38, 1
- Smith, G. & Raggett, D. S. J. 1981, *Journal of Physics B Atomic Molecular Physics*, 14, 4015
- Snedden, C., Cowan, J. J., & Gallino, R. 2008, *ARA&A*, 46, 241
- Snedden, C., Cowan, J. J., Lawler, J. E., et al. 2003, *ApJ*, 591, 936
- Snedden, C., Preston, G. W., McWilliam, A., & Searle, L. 1994, *ApJ*, 431, L27
- Sobeck, J. S., Lawler, J. E., & Sneden, C. 2007, *Astrophys. J.*, 667, 1267
- Spite, M., Andrievsky, S. M., Spite, F., et al. 2012, *A&A*, 541, A143
- Takeda, Y., Hashimoto, O., Taguchi, H., et al. 2005, *PASJ*, 57, 751
- Vidal, C. R., Cooper, J., & Smith, E. W. 1973, *ApJS*, 25, 37
- Whaling, W. & Brault, J. W. 1988, *Phys. Scr*, 38, 707
- Wickliffe, M. E. & Lawler, J. E. 1997a, *Journal of the Optical Society of America B Optical Physics*, 14, 737
- Wickliffe, M. E. & Lawler, J. E. 1997b, *ApJS*, 110, 163
- Wickliffe, M. E., Lawler, J. E., & Nave, G. 2000, *J. Quant. Spec. Radiat. Transf.*, 66, 363
- Wickliffe, M. E., Salih, S., & Lawler, J. E. 1994, *J. Quant. Spec. Radiat. Transf.*, 51, 545
- Wood, M. P., Lawler, J. E., Sneden, C., & Cowan, J. J. 2013, *ApJS*, 208, 27

Table 3. Line data and abundances from an analysis of HE 2252–4225. Γ_6 corresponds to 10 000 K. Column 6 gives references to the adopted gf -values. Column 13 gives references to the sources of the used IS and HFS data and adopted Γ_6 -values.

Z	Atom/ mol	λ (Å)	E_{exc} (eV)	$\log gf$	Ref	$\log \varepsilon$			[X/Fe]	W_λ (mÅ)	$\log \Gamma_6/N_H$ (rad/s·cm ³)	Note, ref.
						Solar	LTE	NLTE				
1	2	3	4	5	6	7	8	9	10	11	12	13
3	Li I	6707.80	0.00	0.167	NIST8	1.10	≤ -0.1			Syn	−7.574	IS:SRE95 Γ_6 :ABO
6	CH	4310-4312.5			BCB05	8.39	5.13		−0.63	Syn		
6	CH	4314			BCB05	8.39	5.16		−0.60	Syn		
6	CH	4362-4364.5			BCB05	8.39	5.14		−0.62	Syn		
6	CH	4366-4367.0			BCB05	8.39	5.16		−0.60	Syn		
7	NH	3416.64		−0.94	K94	7.83	4.91		−0.29	Syn		
11	Na I	5889.96	0.00	0.11	NIST8	6.30	3.57	3.13	−0.54	Syn	−7.67	Γ_6 :ABO
11	Na I	5895.93	0.00	−0.19	NIST8	6.30	3.57	3.13	−0.54	Syn	−7.67	Γ_6 :ABO
12	Mg I	4571.10	0.00	−5.62	NIST8	7.54	4.98	5.22	0.31	Syn	−7.77	Γ_6 :ABO
12	Mg I	4702.99	4.33	−0.44	CT90	7.54	4.98	5.01	0.10	Syn	−6.99	Γ_6 :M13
12	Mg I	5528.41	4.33	−0.50	CT90	7.54	5.02	5.03	0.12	Syn	−7.18	Γ_6 :M13
13	Al I	3961.52	0.01	−0.34	NIST8	6.47	2.85	2.99	−0.85	Syn	−7.32	Γ_6 :ABO
14	Si I	3905.53	1.91	−1.04	BL91	7.52	4.99	4.97	0.08	Syn	−7.36	Γ_6 :ABO
20	Ca I	4425.44	1.88	−0.36	SON75	6.33	3.60	3.86	0.16	36.8	−7.432	Γ_6 :MKP07
20	Ca I	5349.46	2.71	−0.31	SR81	6.33	3.74	4.05	0.35	10.1	−7.652	Γ_6 :S81
20	Ca I	5588.75	2.53	0.36	SR81	6.33	3.62	3.92	0.22	39.5	−7.628	Γ_6 :S81
20	Ca I	5857.45	2.93	0.24	SR81	6.33	3.69	3.87	0.17	17.0	−7.316	Γ_6 :S81
20	Ca I	6122.22	1.89	−0.31	SON75	6.33	3.73	3.96	0.26	53.4	−7.189	Γ_6 :ABO
20	Ca I	6162.17	1.90	−0.09	SON75	6.33	3.70	3.90	0.20	64.5	−7.189	Γ_6 :ABO
20	Ca I	6169.56	2.53	−0.48	SR81	6.33	3.68	3.97	0.27	10.5	−7.264	Γ_6 :S81
20	Ca I	6439.08	2.53	0.39	SR81	6.33	3.65	3.83	0.13	45.6	−7.704	Γ_6 :S81
20	Ca I	6449.81	2.52	−0.50	SR81	6.33	3.69	3.93	0.23	10.6	−7.652	Γ_6 :S81
20	Ca I	6493.78	2.52	−0.11	SR81	6.33	3.70	3.95	0.25	23.3	−7.704	Γ_6 :S81
21	Sc II	3567.70	0.00	−0.48	LD89	3.07	0.39		−0.05	Syn		HFS:MPS95
21	Sc II	4314.09	0.62	−0.10	LD89	3.07	0.31		−0.13	Syn		the same
21	Sc II	4400.39	0.60	−0.54	LD89	3.07	0.26		−0.18	Syn		the same
21	Sc II	4415.56	0.60	−0.67	LD89	3.07	0.31		−0.13	Syn		the same
22	Ti I	3998.64	0.05	0.02	LGW13	4.90	2.21		0.20	67.6	−7.654	Γ_6 :ABO
22	Ti I	4533.25	0.85	0.54	LGW13	4.90	2.22		0.21	50.2	−7.593	the same
22	Ti I	4534.78	0.84	0.35	LGW13	4.90	2.19		0.18	39.1	−7.596	the same
22	Ti I	4981.73	0.85	0.57	LGW13	4.90	2.28		0.27	58.2	−7.626	the same
22	Ti I	4991.06	0.84	0.45	LGW13	4.90	2.29		0.28	53.0	−7.629	the same
22	Ti I	5022.87	0.83	−0.33	LGW13	4.90	2.22		0.21	13.8	−7.633	the same
22	Ti I	5024.85	0.82	−0.53	LGW13	4.90	2.38		0.37	13.1	−7.635	the same
22	Ti I	5039.96	0.02	−1.08	LGW13	4.90	2.31		0.30	25.7	−7.720	the same
22	Ti I	5064.66	0.05	−0.94	LGW13	4.90	2.28		0.27	29.2	−7.719	the same
22	Ti I	5210.39	0.05	−0.82	LGW13	4.90	2.27		0.26	35.5	−7.724	the same
22	Ti II	4028.34	1.89	−0.92	WL13	4.90	2.62		0.36	56.8		
22	Ti II	4053.83	1.89	−1.07	WL13	4.90	2.44		0.17	39.3		
22	Ti II	4394.05	1.22	−1.77	WL13	4.90	2.65		0.38	59.6		
22	Ti II	4395.85	1.24	−1.93	WL13	4.90	2.62		0.35	48.0		
22	Ti II	4399.77	1.24	−1.20	WL13	4.90	2.74		0.47	89.1		
22	Ti II	4417.72	1.16	−1.19	PTP01	4.90	2.76		0.49	94.0		
22	Ti II	4418.33	1.24	−1.99	WL13	4.90	2.64		0.37	45.5		
22	Ti II	4444.56	1.12	−2.20	WL13	4.90	2.71		0.44	46.1		
22	Ti II	4450.48	1.08	−1.52	WL13	4.90	2.73		0.46	83.7		
22	Ti II	4464.45	1.16	−1.81	PTP01	4.90	2.72		0.45	65.1		
22	Ti II	4470.86	1.16	−2.02	PTP01	4.90	2.55		0.28	45.0		
22	Ti II	5185.91	1.89	−1.41	WL13	4.90	2.54		0.27	33.2		
22	Ti II	5188.70	1.58	−1.05	PTP01	4.90	2.70		0.43	82.4		
22	Ti II	5226.55	1.57	−1.26	PTP01	4.90	2.61		0.34	67.8		
22	Ti II	5336.79	1.58	−1.60	WL13	4.90	2.60		0.33	47.2		

Table 3. continued.

Z	Atom/ mol	λ (Å)	E_{exc} (eV)	$\log gf$	Ref	$\log \varepsilon$			[X/Fe]	W_λ (mÅ)	$\log \Gamma_6/N_H$ (rad/s·cm ³)	Note, ref.
						Solar	LTE	NLTE				
1	2	3	4	5	6	7	8	9	10	11	12	13
22	Ti II	5381.01	1.57	−1.97	WL13	4.90	2.60		0.33	28.6		
23	V II	3530.76	1.07	−0.47	BGF89	4.00	1.09		−0.28	Syn		
23	V II	3545.19	1.10	−0.26	BGF89	4.00	1.14		−0.23	Syn		
23	V II	3592.03	1.10	−0.26	BGF89	4.00	1.14		−0.23	Syn		
24	Cr I	5206.04	0.94	0.02	SLS07	5.64	2.62		−0.13	83.6	−7.597	Γ_6 :ABO
24	Cr I	5296.69	0.98	−1.36	SLS07	5.64	2.73		−0.02	17.4	−7.621	the same
24	Cr I	5345.81	1.00	−0.95	SLS07	5.64	2.70		−0.05	32.8	−7.620	the same
24	Cr I	5348.33	1.00	−1.21	SLS07	5.64	2.60		−0.15	17.2	−7.620	the same
24	Cr I	5409.80	1.03	−0.67	SLS07	5.64	2.64		−0.11	42.8	−7.620	the same
24	Cr II	4558.65	4.07	−0.45	PGB93	5.65	3.10		0.08	Syn		
24	Cr II	4588.20	4.07	−0.63	PGB93	5.65	3.08		0.06	Syn		
24	Cr II	4634.07	4.07	−0.98	NLL06	5.65	2.99		−0.03	Syn		
24	Cr II	4848.23	3.86	−1.00	NLL06	5.65	3.01		−0.01	Syn		
25	Mn I	4033.06	0.00	−0.64	DLS11	5.37	2.05		−0.43	Syn	−7.738	HFS:LGB03
25	Mn I	4041.35	2.11	0.28	DLS11	5.37	2.35		−0.13	Syn	−7.701	Γ_6 :ABO
25	Mn I	4055.54	2.13	−0.08	DLS11	5.37	2.44		−0.04	Syn	−7.698	the same
25	Mn I	4823.52	2.32	0.12	DLS11	5.37	2.44		−0.04	Syn	−7.600	the same
25	Mn II	3460.31	1.81	−0.64	KG00	5.37	2.63		−0.11	Syn		HFS:HSR99
25	Mn II	3482.90	1.83	−0.84	KG00	5.37	2.63		−0.11	Syn		the same
25	Mn II	3488.67	1.85	−0.95	KG00	5.37	2.60		−0.14	Syn		the same
26	Fe I	3917.18	0.99	−2.15	OWL91	7.45	4.82	5.04	0.22	91.7	−7.695	Γ_6 :AB
26	Fe I	3949.95	2.18	−1.25	OWL91	7.45	4.60	4.84	0.02	61.8	−7.820	the same
26	Fe I	4132.90	2.85	−1.01	OWL91	7.45	4.57	4.82	0.00	34.9	−7.659	the same
26	Fe I	4147.67	1.49	−2.07	OWL91	7.45	4.70	4.91	0.09	69.5	−7.648	the same
26	Fe I	4216.18	0.00	−3.36	FMW88	7.45	4.86	5.12	0.30	98.8	−7.797	the same
26	Fe I	4260.47	2.40	0.08	OWL91	7.45	4.53	4.70	−0.12	110.0	−7.274	the same
26	Fe I	4445.47	0.09	−5.44	BIP79	7.45	4.79	5.00	0.18	7.5	−7.816	the same
26	Fe I	4602.94	1.49	−2.21	OWL91	7.45	4.65	4.89	0.07	65.6	−7.790	the same
26	Fe I	4647.43	2.95	−1.35	OWL91	7.45	4.67	4.93	0.11	21.0	−7.685	the same
26	Fe I	4920.50	2.83	0.07	OWL91	7.45	4.56	4.75	−0.07	94.8	−7.276	the same
26	Fe I	4966.09	3.33	−0.87	OWL91	7.45	4.67	4.97	0.15	23.2	−7.218	the same
26	Fe I	4994.13	0.92	−2.97	OWL91	7.45	4.67	4.89	0.07	66.6	−7.744	the same
26	Fe I	5001.86	3.88	0.01	FMW88	7.45	4.43	4.73	−0.09	22.9	−7.273	the same
26	Fe I	5014.94	3.94	−0.30	OWL91	7.45	4.65	4.93	0.11	16.8	−7.268	the same
26	Fe I	5051.63	0.92	−2.77	OWL91	7.45	4.82	5.03	0.21	84.1	−7.746	the same
26	Fe I	5068.77	2.94	−1.04	OWL91	7.45	4.55	4.81	−0.01	31.1	−7.265	the same
26	Fe I	5150.84	0.99	−3.04	OWL91	7.45	4.62	4.83	0.01	55.7	−7.742	the same
26	Fe I	5166.28	0.00	−4.20	OWL91	7.45	4.81	5.05	0.23	70.8	−7.826	the same
26	Fe I	5192.34	3.00	−0.42	OWL91	7.45	4.47	4.74	−0.08	57.5	−7.266	the same
26	Fe I	5194.94	1.56	−2.02	OWL91	7.45	4.66	4.86	0.04	75.4	−7.680	the same
26	Fe I	5198.71	2.22	−2.14	BPSS	7.45	4.65	4.87	0.05	25.2	−7.600	the same
26	Fe I	5216.27	1.61	−2.08	OWL91	7.45	4.62	4.81	−0.01	67.0	−7.674	the same
26	Fe I	5217.39	3.21	−1.07	BKK91	7.45	4.51	4.75	−0.07	15.9	−7.220	the same
26	Fe I	5232.94	2.94	−0.06	OWL91	7.45	4.51	4.74	−0.08	82.1	−7.288	the same
26	Fe I	5247.06	0.09	−4.95	BIP79	7.45	4.75	4.98	0.16	22.0	−7.826	the same
26	Fe I	5250.21	0.12	−4.94	BIP79	7.45	4.76	4.98	0.16	21.0	−7.832	the same
26	Fe I	5281.79	3.04	−0.83	OWL91	7.45	4.51	4.78	−0.04	35.0	−7.266	the same
26	Fe I	5283.62	3.24	−0.52	OWL91	7.45	4.61	4.87	0.05	43.7	−7.221	the same
26	Fe I	5324.18	3.21	−0.10	BKK91	7.45	4.43	4.69	−0.13	59.3	−7.235	the same
26	Fe I	5339.93	3.27	−0.72	OWL91	7.45	4.58	4.84	0.02	30.4	−7.221	the same
26	Fe I	5364.87	4.45	0.23	OWL91	7.45	4.65	4.97	0.15	15.7	−7.136	the same
26	Fe I	5367.47	4.41	0.44	OWL91	7.45	4.50	4.84	0.02	18.8	−7.153	the same
26	Fe I	5369.96	4.37	0.54	OWL91	7.45	4.44	4.79	−0.03	22.1	−7.179	the same
26	Fe I	5383.37	4.31	0.64	OWL91	7.45	4.45	4.81	−0.01	30.2	−7.219	the same
26	Fe I	5393.17	3.24	−0.72	BKK91	7.45	4.53	4.79	−0.03	29.8	−7.235	the same
26	Fe I	5410.91	4.47	0.40	OWL91	7.45	4.43	4.77	−0.05	13.5	−7.132	the same
26	Fe I	5415.20	4.39	0.64	OWL91	7.45	4.42	4.80	−0.02	25.0	−7.182	the same
26	Fe I	5434.52	1.01	−2.13	OWL91	7.45	4.79	4.94	0.12	110.0	−7.749	the same

Table 3. continued.

Z	Atom/ mol	λ (Å)	E_{exc} (eV)	$\log gf$	Ref	$\log \varepsilon$			[X/Fe]	W_λ (mÅ)	$\log \Gamma_6/N_H$ (rad/s·cm ³)	Note, ref.
						Solar	LTE	NLTE				
1	2	3	4	5	6	7	8	9	10	11	12	13
26	Fe I	5445.04	4.39	−0.02	FMW88	7.45	4.74	5.06	0.24	13.2	−7.189	the same
26	Fe I	5506.78	0.99	−2.80	OWL91	7.45	4.79	4.98	0.16	80.3	−7.753	the same
26	Fe I	5576.09	3.43	−1.00	FMW88	7.45	4.70	4.94	0.12	16.5	−7.200	the same
26	Fe I	5586.76	3.37	−0.10	BKK91	7.45	4.43	4.68	−0.13	49.9	−7.221	the same
26	Fe I	5615.64	3.33	0.05	BKK91	7.45	4.39	4.64	−0.18	59.0	−7.234	the same
26	Fe I	6065.48	2.61	−1.53	BPS82	7.45	4.62	4.83	0.01	33.8	−7.636	the same
26	Fe I	6136.62	2.45	−1.41	OWL91	7.45	4.65	4.86	0.04	53.0	−7.609	the same
26	Fe I	6137.69	2.59	−1.35	OWL91	7.45	4.60	4.81	−0.01	43.9	−7.589	the same
26	Fe I	6191.56	2.43	−1.42	OWL91	7.45	4.57	4.79	−0.03	50.1	−7.615	the same
26	Fe I	6213.43	2.22	−2.48	OWL91	7.45	4.59	4.81	−0.01	13.6	−7.704	the same
26	Fe I	6252.56	2.40	−1.69	BPSS	7.45	4.66	4.88	0.06	41.3	−7.680	the same
26	Fe I	6393.60	2.43	−1.43	OWL91	7.45	4.50	4.75	−0.07	46.0	−7.622	the same
26	Fe I	6400.00	3.60	−0.29	BKK91	7.45	4.48	4.77	−0.05	30.2	−7.232	the same
26	Fe I	6411.65	3.65	−0.59	BKK91	7.45	4.52	4.79	−0.03	16.9	−7.224	the same
26	Fe I	6421.35	2.28	−2.03	BPSS	7.45	4.66	4.86	0.04	31.9	−7.792	the same
26	Fe I	6430.85	2.18	−1.95	OWL91	7.45	4.59	4.81	−0.01	39.2	−7.704	the same
26	Fe II	4491.40	2.86	−2.71	MB09	7.45	4.80	4.80	−0.02	25.1	−7.880	the same
26	Fe II	4508.29	2.86	−2.44	MB09	7.45	4.88	4.89	0.07	42.4	−7.870	the same
26	Fe II	4582.83	2.84	−3.18	MB09	7.45	4.73	4.73	−0.09	9.5	−7.880	the same
26	Fe II	4620.52	2.83	−3.21	MB09	7.45	4.69	4.70	−0.12	8.6	−7.880	the same
26	Fe II	4923.93	2.89	−1.26	MB09	7.45	4.85	4.82	0.01	98.5	−7.890	the same
26	Fe II	5018.44	2.89	−1.10	MB09	7.45	4.89	4.86	0.04	109.0	−7.890	the same
26	Fe II	5197.58	3.23	−2.22	MB09	7.45	4.84	4.85	0.03	31.4	−7.880	the same
26	Fe II	5234.62	3.22	−2.18	MB09	7.45	4.82	4.83	0.01	33.3	−7.880	the same
26	Fe II	5264.81	3.23	−3.13	MB09	7.45	4.91	4.92	0.10	6.4	−7.880	the same
26	Fe II	5284.11	2.89	−3.11	MB09	7.45	4.85	4.85	0.03	13.5	−7.890	the same
26	Fe II	6247.56	3.89	−2.30	MB09	7.45	4.72	4.74	−0.08	5.3	−7.880	the same
26	Fe II	6456.38	3.90	−2.05	MB09	7.45	4.85	4.87	0.05	11.6	−7.880	the same
27	Co I	3412.33	0.51	0.03	CSS82	4.92	1.91		−0.12	Syn	−7.666	HFS:P96
27	Co I	3489.40	0.92	0.15	CSS82	4.92	2.00		−0.03	Syn	−7.610	Γ_6 :ABO
27	Co I	4121.31	0.92	−0.30	NKW99	4.92	2.08		0.05	Syn	−7.724	the same
27	Co II	3501.72	2.20	−1.00	SLW85	4.92	2.16		−0.13	Syn		the same
28	Ni I	3413.47	0.16	−1.48	FMW88	6.23	3.15		−0.19	Syn	−7.690	Γ_6 :ABO
28	Ni I	3413.93	0.11	−1.72	FMW88	6.23	3.25		−0.09	Syn	−7.785	the same
28	Ni I	3783.52	0.42	−1.31	FMW88	6.23	3.34		0.00	Syn	−7.780	the same
28	Ni I	3807.14	0.42	−1.18	FMW88	6.23	3.45		0.11	Syn	−7.694	the same
28	Ni I	3858.29	0.42	−0.97	FMW88	6.23	3.35		0.01	Syn	−7.700	the same
28	Ni I	5035.37	3.63	0.29	WL97a	6.23	3.51		0.17	Syn	−7.231	the same
28	Ni II	3769.46	3.10	−1.72	K03	6.23	3.75		0.15	Syn		
30	Zn I	4722.16	4.01	−0.37	RL12	4.62	2.43	2.41	0.42	Syn		
30	Zn I	4810.54	4.08	−0.15	RL12	4.62	2.44	2.42	0.43	Syn		
38	Sr II	4077.72	0.00	0.15	RCW80	2.92	0.16	0.23	−0.06	Syn	−7.792	HFS:BBH83
38	Sr II	4215.54	0.00	−0.17	RCW80	2.92	0.16	0.16	−0.13	Syn	−7.792	Γ_6 :MZG08
												HFS:BBH83
												Γ_6 :MZG08
39	Y II	3549.01	0.13	−0.28	HLG82	2.21	−0.36		0.06	Syn		
39	Y II	3600.74	0.18	0.28	HLG82	2.21	−0.56		−0.14	Syn		
39	Y II	3611.04	0.13	0.01	HLG82	2.21	−0.77		−0.35	Syn		
39	Y II	3774.33	0.13	0.21	HLG82	2.21	−0.56		−0.14	Syn		
39	Y II	3788.69	0.10	−0.07	HLG82	2.21	−0.59		−0.17	Syn		
39	Y II	3950.35	0.10	−0.49	HLG82	2.21	−0.55		−0.13	Syn		
39	Y II	4398.01	0.13	−1.00	HLG82	2.21	−0.54		−0.12	Syn		
39	Y II	4883.68	1.08	0.07	HLG82	2.21	−0.62		−0.20	Syn		
39	Y II	5087.43	1.08	−0.17	HLG82	2.21	−0.64		−0.22	Syn		
40	Zr II	3404.83	0.36	−0.49	LNA06	2.58	−0.06		−0.01	Syn		
40	Zr II	3457.56	0.56	−0.47	MBM06	2.58	−0.11		−0.06	Syn		

Table 3. continued.

Z	Atom/ mol	λ (Å)	E_{exc} (eV)	$\log gf$	Ref	$\log \varepsilon$			[X/Fe]	W_λ (mÅ)	$\log \Gamma_6/N_H$ (rad/s·cm ³)	Note, ref.
						Solar	LTE	NLTE				
1	2	3	4	5	6	7	8	9	10	11	12	13
40	Zr II	3479.39	0.71	0.18	LNA06	2.58	0.06		0.11	Syn		
40	Zr II	3481.17	0.80	0.16	CC83	2.58	0.07		0.12	Syn		
40	Zr II	3499.57	0.41	−1.06	LNA06	2.58	0.04		0.09	Syn		
40	Zr II	3505.67	0.16	−0.39	LNA06	2.58	0.09		0.14	Syn		
40	Zr II	3551.95	0.10	−0.36	LNA06	2.58	0.07		0.12	Syn		
40	Zr II	3766.82	0.41	−0.83	LNA06	2.58	0.17		0.22	Syn		
40	Zr II	3991.13	0.76	−0.31	LNA06	2.58	0.06		0.11	Syn		
40	Zr II	3998.97	0.56	−0.52	LNA06	2.58	0.12		0.17	Syn		
40	Zr II	4161.21	0.71	−0.59	LNA06	2.58	0.09		0.14	Syn		
40	Zr II	4208.98	0.71	−0.51	LNA06	2.58	0.12		0.17	Syn		
42	Mo I	3864.11	0.00	−0.01	FW96	1.92	−0.84		0.13	Syn		
44	Ru I	3728.02	0.00	0.27	WSL94	1.84	−0.45		0.60	Syn		
56	Ba II	5853.67	0.60	−1.00	RCW80	2.17	−0.25	−0.27	0.19	Syn	−7.584	Γ_6 :ABO
56	Ba II	6141.71	0.70	−0.08	RCW80	2.17	−0.18	−0.35	0.11	Syn	−7.584	the same
56	Ba II	6496.90	0.60	−0.38	RCW80	2.17	−0.10	−0.33	0.13	Syn	−7.584	the same
57	La II	3849.01	0.00	−0.45	LBS01	1.14	−1.12		0.37	Syn		HFS:LBS01
57	La II	3949.10	0.40	0.49	LBS01	1.14	−1.16		0.33	Syn		the same
57	La II	3988.51	0.40	0.21	LBS01	1.14	−1.15		0.34	Syn		the same
57	La II	3995.74	0.17	−0.06	LBS01	1.14	−1.11		0.38	Syn		the same
57	La II	4077.34	0.24	−0.06	LBS01	1.14	−1.01		0.48	Syn		the same
57	La II	4086.71	0.00	−0.07	LBS01	1.14	−1.14		0.35	Syn		the same
57	La II	4196.55	0.32	−0.30	LBS01	1.14	−1.09		0.40	Syn		the same
57	La II	4920.98	0.13	−0.58	LBS01	1.14	−0.99		0.50	Syn		the same
58	Ce II	3942.15	0.00	−0.22	LSC09	1.61	−0.75		0.27	Syn		
58	Ce II	3992.38	0.45	−0.22	LSC09	1.61	−0.75		0.27	Syn		
58	Ce II	3999.24	0.30	0.06	LSC09	1.61	−0.75		0.27	Syn		
58	Ce II	4073.47	0.48	0.21	LSC09	1.61	−0.72		0.30	Syn		
58	Ce II	4083.22	0.70	0.27	LSC09	1.61	−0.73		0.29	Syn		
58	Ce II	4127.36	0.68	0.31	LSC09	1.61	−0.77		0.25	Syn		
58	Ce II	4137.64	0.52	0.40	LSC09	1.61	−0.74		0.28	Syn		
58	Ce II	4222.60	0.12	−0.15	LSC09	1.61	−0.68		0.34	Syn		
58	Ce II	4486.91	0.30	−0.18	LSC09	1.61	−0.73		0.29	Syn		
58	Ce II	4562.36	0.48	0.21	LSC09	1.61	−0.68		0.34	Syn		
59	Pr II	4179.40	0.20	0.48	ILW01	0.76	−1.23		0.64	Syn		HFS:G89
59	Pr II	4408.82	0.00	0.18	ILW01	0.76	−1.29		0.58	Syn		the same
59	Pr II	4222.93	0.05	0.27	ILW01	0.76	−1.25		0.62	Syn		the same
60	Nd II	3784.25	0.38	0.15	DLS03	1.45	−0.72		0.46	Syn		
60	Nd II	3838.98	0.00	−0.24	DLS03	1.45	−0.68		0.50	Syn		
60	Nd II	3991.74	0.00	−0.26	DLS03	1.45	−0.58		0.60	Syn		
60	Nd II	4018.82	0.06	−0.85	DLS03	1.45	−0.66		0.52	Syn		
60	Nd II	4021.33	0.32	−0.10	DLS03	1.45	−0.69		0.49	Syn		
60	Nd II	4023.00	0.56	0.04	DLS03	1.45	−0.64		0.54	Syn		
60	Nd II	4059.95	0.20	−0.52	DLS03	1.45	−0.71		0.47	Syn		
60	Nd II	4061.08	0.47	0.55	DLS03	1.45	−0.61		0.57	Syn		
60	Nd II	4069.26	0.06	−0.57	DLS03	1.45	−0.56		0.62	Syn		
60	Nd II	4135.32	0.63	−0.07	DLS03	1.45	−0.60		0.58	Syn		
60	Nd II	4156.08	0.18	0.16	DLS03	1.45	−0.56		0.62	Syn		
60	Nd II	4177.33	0.06	−0.10	DLS03	1.45	−0.62		0.56	Syn		
60	Nd II	4232.37	0.06	−0.47	DLS03	1.45	−0.64		0.54	Syn		
60	Nd II	4385.66	0.20	−0.30	DLS03	1.45	−0.64		0.54	Syn		
60	Nd II	4446.38	0.20	−0.35	DLS03	1.45	−0.61		0.57	Syn		
60	Nd II	4462.98	0.56	0.04	DLS03	1.45	−0.56		0.62	Syn		
60	Nd II	4563.22	0.18	−0.88	DLS03	1.45	−0.44		0.74	Syn		
60	Nd II	4706.54	0.00	−0.71	DLS03	1.45	−0.58		0.60	Syn		
60	Nd II	5319.82	0.55	−0.14	DLS03	1.45	−0.62		0.56	Syn		

Table 3. continued.

Z	Atom/ mol	λ (Å)	E_{exc} (eV)	$\log gf$	Ref	$\log \varepsilon$			[X/Fe]	W_λ (mÅ)	$\log \Gamma_6/N_H$ (rad/s·cm ³)	Note, ref.
						Solar	LTE	NLTE				
1	2	3	4	5	6	7	8	9	10	11	12	13
62	Sm II	3993.31	0.04	−0.93	LDS06	1.00	−0.92		0.71	Syn		
62	Sm II	4318.94	0.28	−0.25	LDS06	1.00	−0.89		0.74	Syn		
62	Sm II	4434.32	0.38	−0.07	LDS06	1.00	−0.89		0.74	Syn		
62	Sm II	4467.34	0.66	0.15	LDS06	1.00	−0.91		0.72	Syn		
62	Sm II	4519.63	0.54	−0.35	LDS06	1.00	−0.89		0.74	Syn		
63	Eu II	3819.67	0.00	0.51	LWD01	0.52	−1.31	−1.24	0.87	Syn		HFS:LWD01
63	Eu II	3907.11	0.21	0.17	LWD01	0.52	−1.31	−1.16	0.95	Syn		the same
63	Eu II	4129.72	0.00	0.22	LWD01	0.52	−1.29	−1.20	0.91	Syn		the same
63	Eu II	4205.02	0.00	0.21	LWD01	0.52	−1.28	−1.22	0.89	Syn		the same
64	Gd II	3768.40	0.08	0.21	DLS06	1.11	−0.74		0.78	Syn		
64	Gd II	3796.38	0.03	0.02	DLS06	1.11	−0.71		0.81	Syn		
64	Gd II	4130.37	0.73	0.14	DLS06	1.11	−0.84		0.68	Syn		
64	Gd II	4215.02	0.43	−0.44	DLS06	1.11	−0.79		0.73	Syn		
65	Tb II	3568.51	0.00	0.36	LWC01	0.28	−1.56		0.79	Syn		HFS:LWB01
65	Tb II	3702.85	0.13	0.44	LWC01	0.28	−1.56		0.79	Syn		the same
65	Tb II	3848.73	0.00	0.28	LWC01	0.28	−1.56		0.79	Syn		the same
66	Dy II	3407.80	0.00	0.18	WLN00	1.13	−0.50		1.00	Syn		
66	Dy II	3445.57	0.00	−0.15	WLN00	1.13	−0.57		0.93	Syn		
66	Dy II	3454.32	0.10	−0.14	WLN00	1.13	−0.77		0.73	Syn		
66	Dy II	3460.97	0.00	−0.07	WLN00	1.13	−0.57		0.93	Syn		
66	Dy II	3506.81	0.10	−0.60	WLN00	1.13	−0.62		0.88	Syn		
66	Dy II	3531.71	0.00	0.77	WLN00	1.13	−0.52		0.98	Syn		
66	Dy II	3536.02	0.54	0.53	WLN00	1.13	−0.67		0.83	Syn		
66	Dy II	3538.52	0.00	−0.02	WLN00	1.13	−0.67		0.83	Syn		
66	Dy II	3550.22	0.59	0.27	WLN00	1.13	−0.67		0.83	Syn		
66	Dy II	3563.15	0.10	−0.36	WLN00	1.13	−0.47		1.03	Syn		
66	Dy II	3694.81	0.10	−0.11	WLN00	1.13	−0.65		0.85	Syn		
66	Dy II	3944.68	0.00	0.11	WLN00	1.13	−0.47		1.03	Syn		
66	Dy II	3996.69	0.59	−0.26	WLN00	1.13	−0.57		0.93	Syn		
66	Dy II	4077.96	0.10	−0.04	WLN00	1.13	−0.52		0.98	Syn		
67	Ho II	3416.44	0.08	0.26	LSC04	0.51	−1.24		0.88	Syn		HFS:LSC04
67	Ho II	3456.00	0.00	0.76	LSC04	0.51	−1.40		0.72	Syn		the same
67	Ho II	3796.67	0.00	0.16	LSC04	0.51	−1.23		0.89	Syn		the same
67	Ho II	3810.60	0.00	0.19	LSC04	0.51	−1.30		0.82	Syn		the same
68	Er II	3499.10	0.06	0.29	LSC08	0.96	−0.93		0.74	Syn		
68	Er II	3633.54	0.00	−0.53	LSC08	0.96	−1.08		0.59	Syn		
68	Er II	3692.65	0.06	0.28	LSC08	0.96	−0.83		0.84	Syn		
68	Er II	3729.52	0.00	−0.59	LSC08	0.96	−0.83		0.84	Syn		
68	Er II	3786.84	0.00	−0.52	LSC08	0.96	−0.78		0.89	Syn		
68	Er II	3830.48	0.00	−0.22	LSC08	0.96	−0.88		0.79	Syn		
68	Er II	3896.23	0.06	−0.12	LSC08	0.96	−0.86		0.81	Syn		
68	Er II	3938.63	0.00	−0.52	MCS75	0.96	−0.98		0.69	Syn		
69	Tm II	3462.20	0.00	0.03	WL97b	0.14	−1.81		0.68	Syn		
69	Tm II	3700.26	0.03	−0.38	WL97b	0.14	−1.71		0.78	Syn		
69	Tm II	3701.36	0.00	−0.54	WL97b	0.14	−1.81		0.68	Syn		
69	Tm II	3795.76	0.03	−0.23	WL97b	0.14	−1.74		0.75	Syn		
69	Tm II	3848.02	0.00	−0.14	WL97b	0.14	−1.74		0.75	Syn		
70	Yb II	3694.19	0.00	−0.30	BDM98	0.86	−0.91		0.86	Syn		HFS:MGH94
76	Os I	4260.85	0.00	−1.43	IAN03	1.45	−0.44		1.00	Syn		
77	Ir I	3513.630	0.00	−1.21	IAN03	1.38	−0.25		1.26	Syn		HFS:CSB05
77	Ir I	3800.120	0.00	−1.44	IAN03	1.38	−0.39		1.12	Syn		HFS:CSB05
82	Pb I	4057.81	1.32	−0.17	BGP00	2.00	≤ −0.78	≤ −0.37	≤ 0.26	Syn		

Table 3. continued.

Z	Atom/ mol	λ (Å)	E_{exc} (eV)	$\log gf$	Ref	$\log \varepsilon$			[X/Fe]	W_λ (mÅ)	$\log \Gamma_6/N_H$ (rad/s·cm ³)	Note, ref.
						Solar	LTE	NLTE				
1	2	3	4	5	6	7	8	9	10	11	12	13
90	Th II	3741.18	0.19	−0.17	NZL02	0.08	−1.65	−1.55	1.00	Syn		
90	Th II	4019.13	0.00	−0.23	NZL02	0.08	−1.62	−1.56	0.99	Syn		

ABO	Anstee & O’Mara (1995), Barklem & O’Mara (1997), Barklem et al. (1998); Barklem & O’Mara (1998), Barklem & Aspelund-Johansson (2005); Barklem (2012, private comm.);
BBH83	Borghs et al. (1983);
BCB05	Barklem et al. (2005);
BDM98	Biémont et al. (1998);
BGF89	Biemont et al. (1989);
BGP00	Biémont et al. (2000);
BIP79	Blackwell et al. (1979);
BKK91	Bard et al. (1991);
BL91	O’brian & Lawler (1991);
BPSS	Blackwell et al. (1982a);
BPS82	Blackwell et al. (1982b);
CC83	Cowley & Corliss (1983);
CSB05	Cowan et al. (2005);
CSS82	Cardon et al. (1982);
CT90	Chang & Tang (1990);
DLS03	Den Hartog et al. (2003);
DLS06	Den Hartog et al. (2006);
DLS11	Den Hartog et al. (2011);
FMW88	Fuhr et al. (1988);
FW96	Fuhr & Wiese (1992);
G89	Ginibre (1989);
HLG82	Hannaford et al. (1982);
HSR99	Holt et al. (1999);
IAN03	Ivarsson et al. (2003);
ILW01	Ivarsson et al. (2001);
K94	Kurucz (1994);
K03	Kurucz (2003);
KG00	Kling & Griesmann (2000);
LBS01	Lawler et al. (2001a);
LD89	Lawler & Dakin (1989);
LDS06	Lawler et al. (2006);
LGB03	Lefèbvre et al. (2003);
LGW13	Lawler et al. (2013);
LNA06	Ljung et al. (2006);
LSC04	Lawler et al. (2004);
LSC08	Lawler et al. (2008);
LSC09	Lawler et al. (2009);
LWB01	Lawler et al. (2001d);
LWC01	Lawler et al. (2001b);
LWD01	Lawler et al. (2001c);
M13	Mashonkina (2013);
MB09	Meléndez & Barbuy (2009);
MBM06	Malcheva et al. (2006);
MCS75	Meggers et al. (1975);
MGH94	Mårtensson-Pendrill et al. (1994);
MKP07	Mashonkina et al. (2007a);
MPS95	McWilliam et al. (1995);
MZG08	Mashonkina et al. (2008);
NIST8	Ralchenko et al. (2008);
NKW99	Nitz et al. (1999);
NLL06	Nilsson et al. (2006);
NZL02	Nilsson et al. (2002);
OWL91	O’brian & Lawler (1991);
P96	Pickering (1996);
PGB93	Pinnington et al. (1993);
PTP01	Pickering et al. (2001);
RCW80	Reader et al. (1980);
RL12	Roederer & Lawler (2012);
S81	Smith (1981);
SLS07	Sobeck et al. (2007);
SLW85	Salih et al. (1985);
SR81	Smith & Raggett (1981);
SON75	Smith & O’Neill (1975);
SRE95	Sansonetti et al. (1995);
WB88	Whaling & Brault (1988);
WL13	Wood et al. (2013);
WL97a	Wickliffe & Lawler (1997b);
WL97b	Wickliffe & Lawler (1997a);
WLN00	Wickliffe et al. (2000);
WSL94	Wickliffe et al. (1994);